



A 9 Month Hubble Space Telescope Near-UV Survey of M87. I. Light and Color Curves of 94 Novae, and a Redetermination of the Nova Rate*

Michael M. Shara¹ , Alec M. Lessing² , Rebekah Hounsell^{3,4} , Shifra Mandel⁵ , David Zurek¹ , Matthew J. Darnley⁶ , Or Graur^{1,7} , Yael Hillman⁸ , Eileen T. Meyer⁹ , Joanna Mikolajewska¹⁰ , James D. Neill¹¹ , Dina Prialnik¹² , and William Sparks¹³

¹ Department of Astrophysics, American Museum of Natural History, New York, NY 10024, USA; mshara@amnh.org

² Department of Physics, Stanford, CA 94305, CA, USA

³ University of Maryland Baltimore County, 1000 Hilltop Circle, Baltimore, MD 21250, USA

⁴ NASA Goddard Space Flight Center, Greenbelt, MD 20771, USA

⁵ Department of Astronomy, Columbia University, New York City, NY 10024, USA

⁶ Liverpool John Moores University, Astrophysics Research Institute, Liverpool L3 5UG, UK

⁷ University of Portsmouth, Institute of Cosmology and Gravitation, Portsmouth PO1 2UP, UK

⁸ Technion—Israel Institute of Technology, Department of Physics, Haifa 3200003, Israel

⁹ University of Maryland Baltimore County, Department of Physics, Baltimore, MD 21250, USA

¹⁰ Nicolaus Copernicus Astronomical Center, Warsaw, 00-716, Poland

¹¹ California Institute of Technology, Division of Physics, Math & Astronomy, Pasadena, CA 91125, USA

¹² Tel Aviv University, Department of Earth and Planetary Sciences, Ramat Aviv, 6997801 Israel

¹³ SETI Institute, Mountain View, CA 94043, USA

Received 2023 August 28; revised 2023 October 4; accepted 2023 October 9; published 2023 November 17

Abstract

M87 has been monitored with a cadence of 5 days over a span of 9 months through the near-ultraviolet (NUV; F275W) and optical (F606W) filters of the Wide Field Camera 3 (WFC3) of the Hubble Space Telescope. This unprecedented dataset yields the NUV and optical light and color curves of 94 M87 novae, characterizing the outburst and decline properties of the largest extragalactic nova dataset in the literature (after M31 and M81). We test and confirm nova modelers' prediction that recurrent novae cannot erupt more frequently than once every 45 days, show that there are zero rapidly recurring novae in the central $\sim 1/3$ of M87 with recurrence times < 130 days, demonstrate that novae closely follow the K -band light of M87 to within a few arcsecs of the galaxy nucleus, show that nova NUV light curves are as heterogeneous as their optical counterparts, and usually peak 5–30 days after visible light maximum, determine our observations' annual detection completeness to be 71%–77%, and measure the rate R_{nova} of nova eruptions in M87 as $352^{+37}_{-37} \text{ yr}^{-1}$. The corresponding luminosity-specific classical nova rate for this galaxy is $7.91^{+1.20}_{-1.20} \text{ yr}/10^{10} L_{\odot,K}$. These rates confirm that ground-based observations of extragalactic novae miss most faint, fast novae and those near the centers of galaxies. An annual M87 nova rate of 300 or more seems inescapable. A luminosity-specific nova rate of $\sim 7\text{--}10 \text{ yr}/10^{10} L_{\odot,K}$ in *all* types of galaxies is indicated by the data available in 2023.

Unified Astronomy Thesaurus concepts: Classical novae (251); Giant elliptical galaxies (651)

Supporting material: figure set, machine-readable tables

1. Introduction and Motivation

All cataclysmic variables (CVs) are binaries containing a white dwarf (WD), which accretes matter from a close companion. A nova eruption is a luminous (up to $10^6 L_{\odot}$) transient that erupts when the envelope accreted onto the WD's surface undergoes a thermonuclear runaway. The recurrence rate, peak luminosity, and brightness decay timescale of a nova depend on the WD mass and the binary mass transfer rate during the time (usually millennia) between nova eruptions (Yaron et al. 2005; Hillman et al. 2016, 2020; Hillman 2021), as well as the chemical compositions of the two stars.

Novae are our only means of detecting and studying CV populations (and indeed most binary populations except for X-ray binaries) in galaxies beyond the Local Group. Differences in CV populations in different types of galaxies would indicate different binary fractions and/or stellar evolution pathways. Additionally, very rapidly accreting WDs in nova binaries can give rise to exploding WD *standard candle* type Ia supernovae (Maoz et al. 2014; Hillman et al. 2016; Jha et al. 2019; Liu et al. 2023). Thus, the importance of CVs extends beyond the field of binary star formation and evolution to cosmology.

Despite CVs' importance, a lack of consensus on one of the most basic parameters that characterize them—the annual nova eruption rates in galaxies—has persisted for two decades. Shafter et al. (2000, 2014, 2021) claimed that the luminosity-specific nova rates (LSNRs; i.e., the annual rate of novae per unit K -band luminosity) in different galaxy types are all similar, $\sim 1\text{--}3 \text{ novae}/\text{yr}/10^{10} L_{\odot,K}$ (solar luminosities in the K band). This conclusion is based on relatively time-sparse, ground-based optical surveys of multiple galaxies, most recently summarized in Shafter et al. (2021).

* This paper is respectfully dedicated to Jay Gallagher and the late Art Code, who first characterized the striking ultraviolet behavior of a nova a half-century ago.



Original content from this work may be used under the terms of the [Creative Commons Attribution 4.0 licence](https://creativecommons.org/licenses/by/4.0/). Any further distribution of this work must maintain attribution to the author(s) and the title of the work, journal citation and DOI.

Population synthesis studies of Matteucci et al. (2003), Claeys et al. (2014), and Chen et al. (2016) predicted a very different behavior: spiral, and especially starburst galaxies, should exhibit an order-of-magnitude higher nova rates and LSNR than elliptical galaxies. This is because newborn binaries containing high-mass WDs should be most common in spiral and starburst galaxies characterized by recent massive star formation. Novae that erupt on those high-mass WDs need only accrete relatively low-mass envelopes in order to initiate thermonuclear runaways (Shara 1981; Yaron et al. 2005); hence, they outburst more frequently than those associated with the mostly low-mass WDs in the nova binaries of elliptical galaxies.

A daily imaging Hubble Space Telescope (HST)-based survey of the massive elliptical galaxy M87 (Shara et al. 2016), spanning 72 days, showed that ground-based surveys of external galaxies fail to detect fainter novae, those with short decline times, and those near the bright centers of galaxies. *These effects cause ground-based surveys to systematically and significantly underestimate the true nova rates in galaxies.* The HST-determined LSNR of M87 has been shown to be $7.88^{+2.3}_{-2.6}$ novae/yr/ $10^{10}L_{\odot,K}$ (Shara et al. 2016). This is two to four times larger than previous ground-based surveys' results. Mróz et al. (2016) demonstrated that the LSNR in the Large Magellanic Cloud (LMC) is much higher than previous ground-based estimates, thereby confirming that it is comparable to the M87 LSNR. De et al. (2021) discovered a sizeable population of Galactic novae (in the infrared) that have gone undetected in over a century of optical searches, and Kawash et al. (2021) found that approximately half of all Galactic novae are hidden by extinction from current surveys. Most recently, Mandel et al. (2023) used a year-long HST survey of M51 to determine its nova rate to be 172^{+46}_{-37} novae yr $^{-1}$, corresponding to an LSNR of $10.4^{+2.8}_{-2.2}$ novae yr $^{-1}/10^{10}L_{\odot,K}$. Both of these rates are $\sim 10\times$ larger than the ground-based-determined nova rates for M51 (Shafter et al. 2000).

These discoveries (of much higher than previously claimed LSNR) in a giant elliptical (M87), a barred spiral (the Galaxy), a dwarf irregular galaxy (the LMC), and a giant Sc-type spiral galaxy (M51) were carried out via surveys with much longer baselines, denser time coverage, and/or deeper magnitude limits than all previous surveys. They argue strongly against the claim that the LSNR is relatively low ($\sim 1\text{--}3$ novae/yr/ $10^{10}L_{\odot,K}$) in all galaxies, as the earlier, shallower, and sparser cadence coverage suggested.

HST is especially well suited to detecting extragalactic novae because of its unparalleled angular resolution and consequent sensitivity, its very small and nearly constant point-spread function (PSF), its insensitivity to the lunar phase, and its immunity to atmospheric seeing. In addition, HST operates effectively in the near-ultraviolet (NUV), a property that has only rarely been exploited in extragalactic nova searches (Sohn et al. 2006; Madrid et al. 2007). Novae erupting on WDs with masses $\gtrsim 1.0 M_{\odot}$ are expected to be NUV bright (Hillman et al. 2014), and NUV observations greatly suppress the light of red giants, which dominate the optical output of elliptical galaxies, so that novae even near ellipticals' bright cores should be detectable in the NUV.

Motivated by the high nova rate in M87 that only HST could have determined, we applied for and were awarded 53 HST orbits (GO-14618, PI: M. Shara) to survey that galaxy for

transients with a 5 day cadence for 9 months. Among the questions we proposed to answer were:

1. Do novae continue to follow the light of M87 all the way to the galaxy nucleus? Would a definitive measurement of the M87 nova rate, using an optimal set of filters (both NUV and visible) change the remarkably high rate?

A nonoptimal (for novae) choice of filters (F814W and F606W, chosen for detecting microlensing in M87) meant that even the Shara et al. (2016) HST survey of M87 for novae is incomplete within $20''$ of its bright nucleus.

2. How do the NUV light curves differ from the optical light curves of novae? What is the distribution of time differences of maximum luminosity in NUV and visible light? Are these correlated with other nova properties?

Only nine UV nova light curves have ever been observed: one via the Orbiting Astronomical Observatory (Gallagher & Code 1974) and eight via the Galaxy Evolution Explorer (GALEX) satellite (Cao et al. 2012). In groundbreaking work a half-century ago, the nova FH Serpentis was shown to brighten in NUV light much later than in the optical (Gallagher & Code 1974), while four decades later Cao et al. (2012) detected two novae in M31 (eight with visual and NUV light curves) that achieved peak brightness in the NUV *before* visible maximum. Theoretical UV (and optical) light curves have been published (Hillman et al. 2014), but no large-scale test of them has been possible due to the paucity of observed NUV nova light curves. Extrapolating from Shara et al. (2016), of order 100 NUV nova light curves should emerge from a 9 month HST survey.

3. Do ultra-rapidly recurring novae exist?

Hillman et al. (2015)'s models of the most massive, rapidly accreting WDs ($1.399 M_{\odot}$ accreting near the Eddington limit) predict that novae can never recur more frequently than once every 45 days, and that such rapidly recurring novae are extremely NUV bright. The 260 day baseline of 5 day cadence observations of M87 of GO-14618 is sufficient to detect any such ultra-rapidly recurring novae multiple times, which would be a serious challenge to the theory and models of novae.

Section 2 describes the data collected during the M87 HST observing campaign. In Section 3, we describe our searches for and identifications of nova candidates and their properties. We derive the nova rate in M87 in Section 4, where we compare it to previous measurements. In Section 5, we place constraints on the possible incidence of the most rapidly recurring novae. We use our large sample of novae to contrast their NUV and optical behaviors in Section 6. We present our other findings in Sections 7 and 8, and summarize our results in Section 9. In the Appendix, we present the tabular data that describes all 94 novae, display a montage of the field of each nova in each filter at each epoch, and the corresponding light and color curves of all of the novae of this study.

2. HST Imaging Data

The HST observing campaign of M87 (Proposal ID: 14618; PI: Shara) was conducted over the course of 260 days using the Wide Field Camera 3 (WFC3) F275W and F606 filters (hereafter U and V respectively). The first observations were taken on 2016 November 13, with the last completed on 2017 July 31. During each of the 53 epochs HST was scheduled to observe the center of M87 for a total 720 s exposure in the F606W filter and 1500 s in the F275W filter; just a few epochs were 1%–3% shorter in exposure time. Figure 1 shows the HST

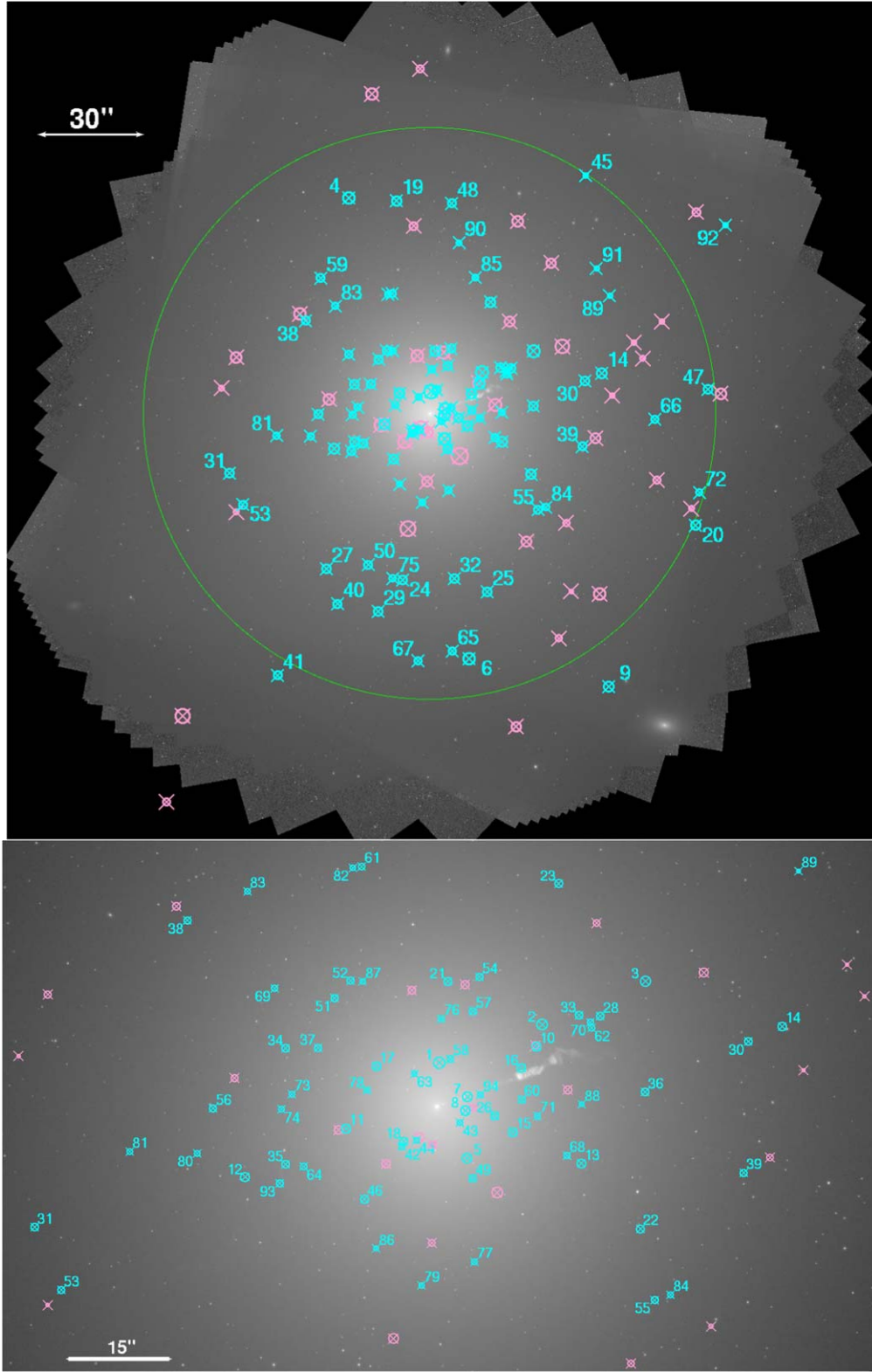


Figure 1. Top: the FOV of 53 HST pointings, and locations (cyan crosses) of all 94 novae detected in M87. North is up and east is left. Also shown as pink crosses are the 32 *certain* novae of Shara et al. (2016). The size of each nova’s circle scales linearly with the brightest observed F606W magnitude of that nova. Markers for novae whose peaks were not observed do not have a circle. The region encompassed by the large green circle is the inner circle defined in Section 2 and used throughout the paper. Bottom: a close-up of the nuclear region of M87 and its novae.

fields of view (FOV) of those 53 epochs. Note that the FOV rotates to maintain optimal pointing of HST’s solar panels throughout the course of the year. Because of this rotation, some novae were rotated into or out of the HST FOV during

their eruptions, and some novae were almost certainly entirely missed (see Section 4). We refer to the area within $81''.1$ (the half-width of the WFC3 UVIS chip) of M87’s nucleus as the *inner circle* (see Figure 1).

The survey’s magnitudes are on the *STAG* system. All absolute magnitudes were computed using an M87 distance modulus of 31.03 (de Grijs & Bono 2019) with Galactic extinction in the direction of M87 of $A_{606} = 0.05$ and $A_{275} = 0.12$ mag (Cardelli et al. 1989; Harris 2009).

3. M87 Nova Search and Identification

We independently conducted two separate searches for novae in the 53 images of the epochs of M87: a search based on visual inspection of difference images and a search based on statistical classification of photometric results.

3.1. Difference Images

All WFC3/UVIS data were reduced using the STScI *calwf3* pipeline (Dressel 2019). Individual FLC exposures were aligned and combined using Dizzlepacs’s *astrodrizzle* package to create individual DRC epoch images in each filter. All images were aligned to the same WCS and pixel scale to easily enable comparison and subtraction.

Next, template epochs were established using combined DRC data at both early and late times during the observation cycle. These images were then subtracted from each epoch DRZ image and the resultant subtracted images were used to search for nova events.

The search for novae from the subtracted dataset was conducted both manually via visual inspection and via the use of SExtractor (Bertin & Arnouts 1996). This resulted in the detection of 125 nova candidates.

3.2. Statistical Method

The statistical search proceeded in multiple steps. First, we used *astrodrizzle* to combine all FLC images of a given filter in a given epoch (so-called epoch 1 images) or a set of three subsequent epochs (so-called epoch 3 images). Additionally, we created median images of all the data from all epochs in each filter. For each use of *astrodrizzle*, we used its cosmic-ray cleaning functionality to eliminate cosmic rays. Other preliminary targets for photometry were identified running DAOFIND with liberal rejection criteria on all drizzled images. Due to the strong gradient in the background because of the presence of M87 in the images, 10 annuli centered on M87’s center were created. For each image, and for each annulus, an average sky standard deviation was calculated and used for the DAOFIND statistical significance criteria for detection within that annulus. This process yielded 27,061 detected sources, most of which were globular clusters, giant stars within M87, resolved features of M87, background galaxies, random statistical fluctuations of the background, and residual noise or cosmic rays.

On each of these targets, we used PyRAF’s PHOT function to measure magnitudes in epoch 1 and epoch 3 images in both filters. We applied a differential correction to photometric measurements of three epochs, finding the average change in magnitude of the hundred nearest sources of similar magnitude to every source and subtracting out overall fluctuations from each source’s light curve. We then calculated an average statistical variation σ in the magnitude of each light curve. To find transients, light curves with either F606W or F275W peak magnitudes greater than 3σ above the median in one passband or 2σ in both passbands were selected as candidates. This eliminated the vast majority of candidates. Each remaining

candidate was examined by eye to eliminate remaining noise or cosmic-ray events. These were evident through highly irregular or resolved PSFs upon visual examination, or large differences in the magnitudes measured in FLC images from the same epoch and passband. This left a list of 122 candidate novae.

3.3. Combined List of Novae

The lists from the two different search methods were then combined, yielding a total of 151 candidates. We then closely inspected each of these, eliminating candidates that only appeared in a single image (in one band and epoch) that had irregular PSFs, were too dim to be confident of photometric statistical significance given local background characteristics, particularly those candidates that only appeared in one epoch, or had light-curve or color characteristics inconsistent with being a nova. This left the final list of 94 novae presented in this paper.

There was excellent overlap between the lists generated by visual inspection of difference images and the statistical method, suggesting detection efficiency near the limit of what is possible with the dataset. Of the final 94 novae, 89 were found using visual inspection of difference images and 91 were found using the statistical method. Notably, the statistical method failed to detect a few novae very close to M87’s jet, whereas difference imaging missed a few novae close to M87’s bright nucleus.

The locations of all 94 novae (and those of 32 certain novae from the Shara et al. 2016 survey) are shown in Figure 1. The log of observations is given in Table 1. The positions, magnitudes, colors, and rates of decline of the novae are listed in Table 2, and photometric measurements are presented in Table 3.

4. M87 Nova Rate

To measure the nova rate in M87, we must first determine our survey’s incompleteness: the fraction of novae that erupted within HST’s FOV in M87 during our survey but which were not detected. Peak luminosity, decline time, and the *shape* of a nova light curve all play a significant role in an individual nova’s detectability, as demonstrated in Figures 5 and 6 of Mandel et al. (2023). The rates of change in luminosity as well as the shapes of light curves vary significantly among well-sampled Galactic novae (Strope et al. 2010). Thus, the regularly spaced epochs of this survey must be convolved with a set of realistic light curves, representative of M87 novae, to determine our survey’s incompleteness, as described below.

4.1. Limiting Magnitudes of Detectable M87 Novae

To determine a detectability criterion for our simulations we estimated a cutoff magnitude, fainter than which a nova would not reliably be considered observable (visually distinguishable from noise) to a human inspector in a given epoch, in both the F606W and F275W bandpasses, as a function of distance from M87’s center. The distribution of light in M87 is close to radially symmetric (Harris & Petrie 1978) within a few arcminutes of M87’s core (which covers our entire FOV), so its Galactic radius can be calibrated as a good proxy for local limiting magnitude. We plotted the dimmest and brightest magnitudes, as measured through aperture photometry, at which our human inspector marked each nova as detectable and nondetectable as a function of radial distance (see Figure 2). At

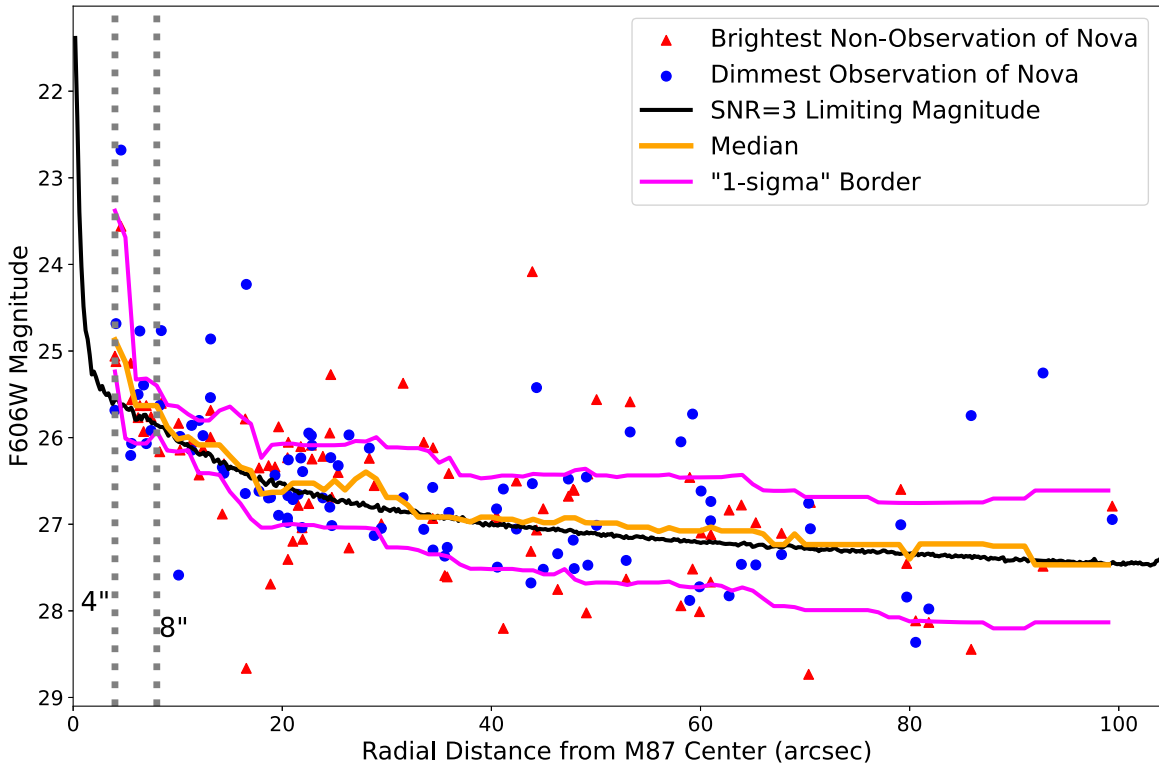


Figure 2. The dimmest F606W magnitude (blue-filled circle) at which each of the 94 M87 novae was observable via direct inspection of the epoch 1 images and the brightest magnitude (red-filled triangle) where each was not observable. The median (orange curve) and 1σ (15.9th and 84.1th) percentiles (magenta lines) of these points are plotted as a function of radial distance. Also plotted (the black curve) is the magnitude of a point source that would have $S/N = 3$ given the average local background noise measured in the F606W epoch 1 images at a given radial distance from the Galactic Center. The $S/N = 3$ line is observed to match the median line well outside of the inner $8''$. See the text for details.

a given radius, the central magnitude at which the distributions of the two sets of points overlapped was taken as an estimate for the local limiting magnitude by the confident human detectability criterion, which is the ultimate criterion we used in the real survey. Outside the inner $8''$ from the nucleus, the local signal-to-noise rate $S/N = 3$ limiting magnitude as a function of radius approximated the center of the overlap region well. This limiting magnitude was computed by measuring the image background noise as a function of distance from the Galactic Center and determining the magnitude of a point source that would have an S/N of 3 when placed upon that background.

Inspection of Figure 2 and examination of the epoch 1 images showed that the $S/N = 3$ curve overestimated the local human detection cutoff magnitude closer than $8''$ from M87's nucleus. This is likely due to the effects of the very strong gradient of the M87 Galactic background on the PSFs of stars very near the Galactic Center. Accordingly, we defined the $S/N = 3$ line as the simulation cutoff magnitude outside $8''$, while between $4''$ and $8''$ we estimated the cutoff based on empirical detection/nondetection of novae. The inner $3''$ – $4''$ of M87 novae are nearly undetectable with the current dataset.

4.2. Placement of Simulated Novae

We selected coordinates for simulated novae within the area of our study's footprint where the detectability of novae could be quantified—inside the inner circle region (shown in Figure 1) with a radius of 2048 WFC3 pixels, or half the detector's width, from M87's center and outside $4''$ from M87's center. Coordinates were sampled with probabilities proportional to M87's local Two Micron All Sky Survey *K*-band

surface brightness, in accordance with the observation that the distribution of novae closely follows the *K*-band light in M87 (Shara et al. (2016) and see below).

4.3. Nova Template Light Curves

While exquisitely detailed light curves exist for hundreds of Galactic novae, observational bias results in very few faint, fast novae (Kasliwal et al. 2011) being included in the Galactic sample. Over 1000 novae have been detected in M31, and excellent visible light curves of novae there include very long-duration, faint novae, and faint, fast novae (Kasliwal et al. 2011). A remarkable $\sim 50\%$ of the Kasliwal et al. (2011) M31 novae are of the faint, fast variety, and these novae are also ubiquitous in M87 (Shara et al. 2016). To be conservative we drew the 59 best-sampled template light curves for our simulation from the Mandel et al. (2023) compilation of best-sampled M31 novae, which are mostly bulge novae and include only $\sim 21\%$ faint, fast novae. (Our nova detection completeness fraction, used to derive the M87 nova rate is weakly dependent on the faint, fast nova fraction that we adopt; a 50% adopted faint, fast nova fraction would have led to a few percent higher incompleteness fraction, and an 8% higher deduced nova rate, as shown in Figure 3.) We corrected the 59 nova light curves to the distance and reddening of M87 (Shara et al. 2016). Light curves were discarded if they had less than 20 days of complete data and/or did not reach as faint as an F606W magnitude of 26.5. We used g , r , and m_{pg} light curves, and assumed that novae have colors close enough to 0.0 (van den Bergh & Younger 1987; Shara et al. 2016) that we could use these data to simulate M87 nova F606W light curves.

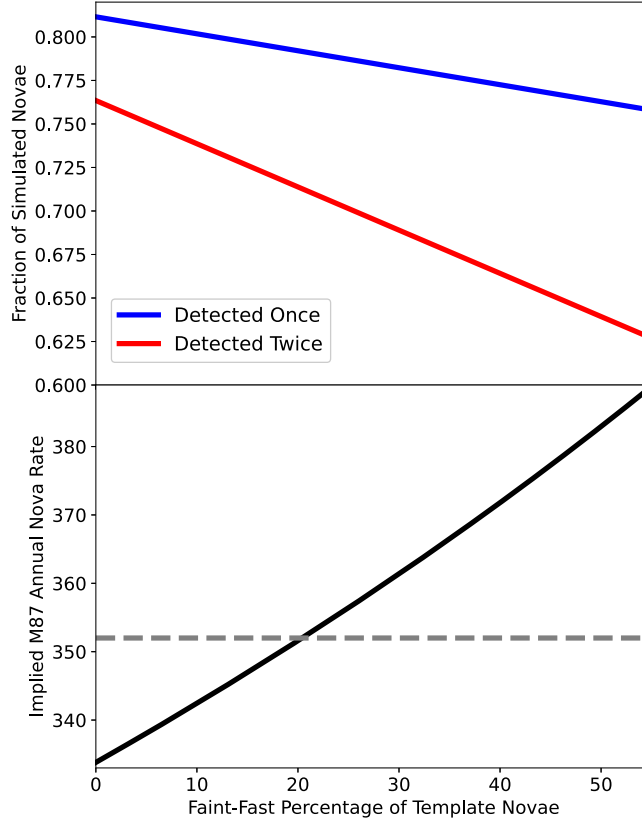


Figure 3. Top: the fraction of simulated novae detected once (blue) and twice (red) in F606W as a function of the percentage of template novae that are faint, fast ($t_2 < 10$ days and peak $M(\text{F606W}) < -7$). Bottom: the annual nova rate for the entirety of M87 implied by the recovery fraction, following the procedure of Section 4.5. Also shown (horizontal line) is the annual nova rate adopted in Section 4.5.

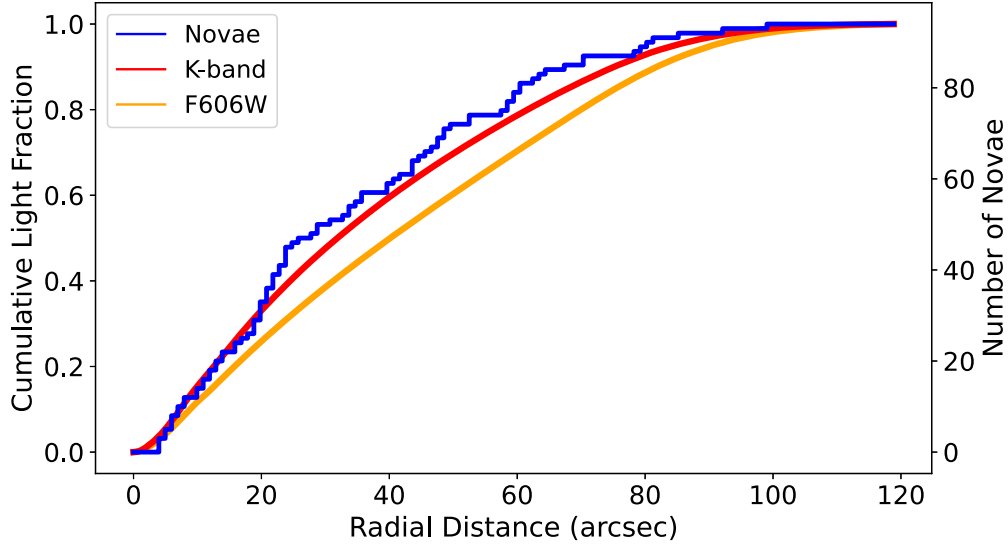


Figure 4. The normalized radial distributions of 94 M87 novae, and the K -band and F606W-band light of the galaxy. The novae are seen to closely track the galaxy K -band light. This is confirmed by the K-S test, which returns the statistic $p = 0.61$.

4.4. Detection Fractions

Each of 500,000 simulated novae was randomly assigned both a template light curve and a day of peak brightness during a 1 yr interval beginning 80 days before the start of our survey’s 260 day window. The template light curves were used to determine the magnitude of each simulated nova in each of the 53 epochs. Simulated novae were deemed *detectable* in a

given epoch if they were brighter than the local cutoff magnitude (see Section 4.1 and Figure 2).

71.1% of simulated novae in the surveyed M87 area were detectable in at least two visible epochs. A further 8.0% were detectable in precisely one visible epoch; this would have warranted exclusion as a nova candidate under our real survey’s criterion that a nova be observed at least twice (see Section 3.3). Using our own nova F275W + F606W light

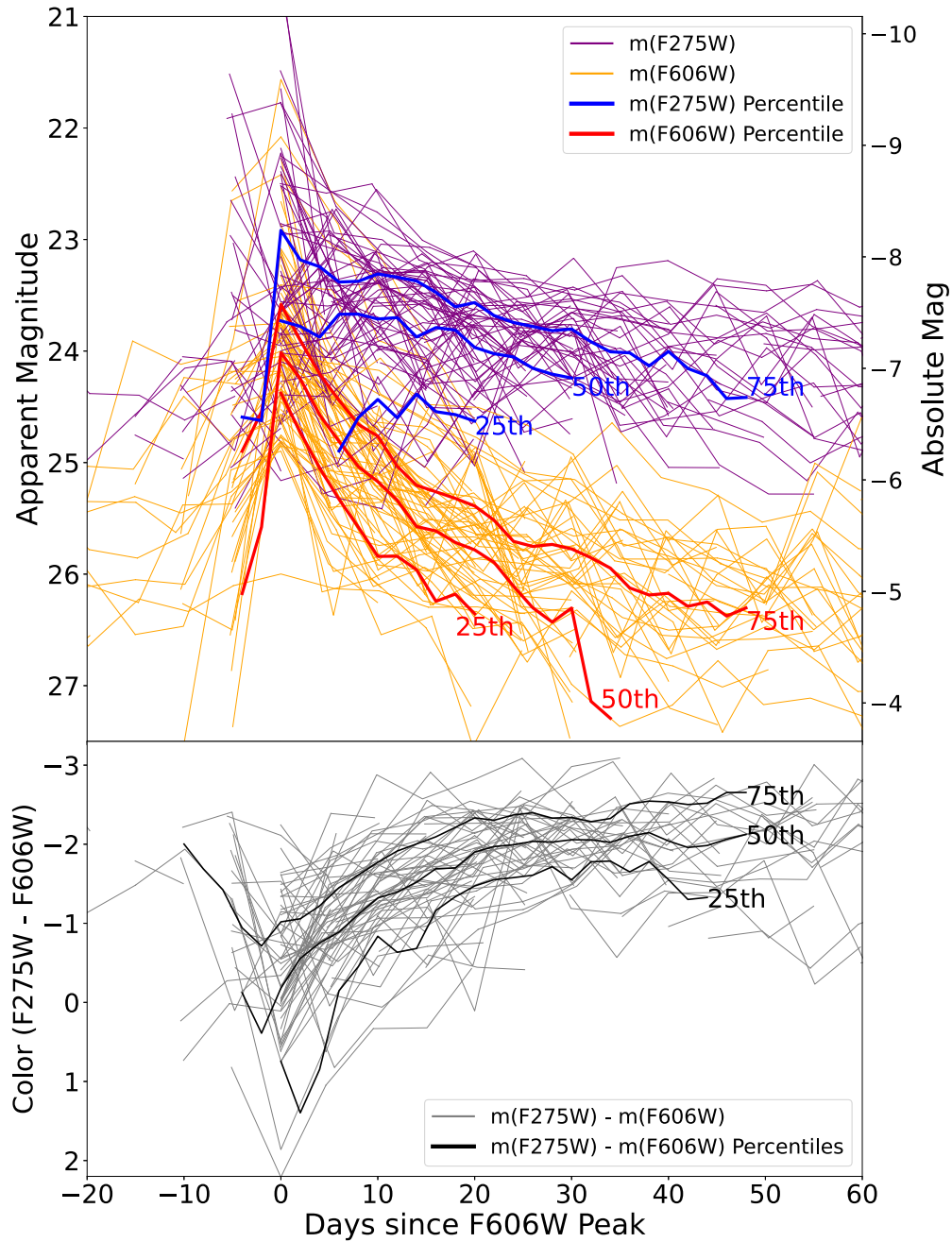


Figure 5. Top: F275W and F606W light curves (purple and orange, respectively) of 77 novae with observed brightness peaks in M87. Over-plotted are the 25th, 50th, and 75th percentiles (in order of brightness) of all of these F275W (in blue) and F606W (in red) light curves. Note that the computation of a percentile at a given time takes into account upper limit magnitude data points in individual nova light curves. To avoid clutter in this plot, those individual limit data points are not shown, but they can be seen in Table 3 and as arrows in Figure 15. The higher luminosities and slower rates of decline of novae in the NUV are apparent. Bottom: the F275W–F606W color curves of the M87 novae, as well as the 25th, 50th, and 75th percentiles of the color curves. Novae near maximum light exhibit $m(\text{F275W}) - m(\text{F606W}) \sim 0 \pm 1$, then become increasingly blue during the ensuing ~ 30 days. After ~ 30 days they remain at $m(\text{F275W}) - m(\text{F606W}) \sim -2 \pm 0.5$.

curves as templates for this 8.0% of once-only detected novae, we estimate $\sim 75\%$ to have also been detectable at least once in the NUV (and thereby to have been confirmable using our real survey’s *seen twice* criterion), for an overall annual detection fraction of $71.1\% + 75\% \times 8.0\% = 77.1\%$. We also note that 95.8% of novae that peaked during the 260 day survey window were detected.

4.5. M87 Nova Rate

The simulations described in Section 4 indicate that between 71.1% and 77.1% of nova eruptions in a 1 yr interval, inside the

inner circle and further than $4''$ from the nucleus, were detected. Of the 94 novae detected in our survey, 90 were in this region.

To model the actual number of novae that peaked in this region in the 1 yr interval, given that 90 were detected with a detection rate between 71.1% and 77.1%, we consider how many novae would have to have peaked in order for us to have detected 90. This quantity is modeled by a $\Gamma(90, .711 \text{ or } .771)$ random variable, which implies that with 68.2% (1σ) confidence, the average annual nova rate in the inner circle and outside $4''$ is between $116.7^{+12.3}_{-12.3}$ and $126.5^{+13.3}_{-13.3}$. We adopt a simple average of these two rates, $121.6^{+12.8}_{-12.8}$, as our best

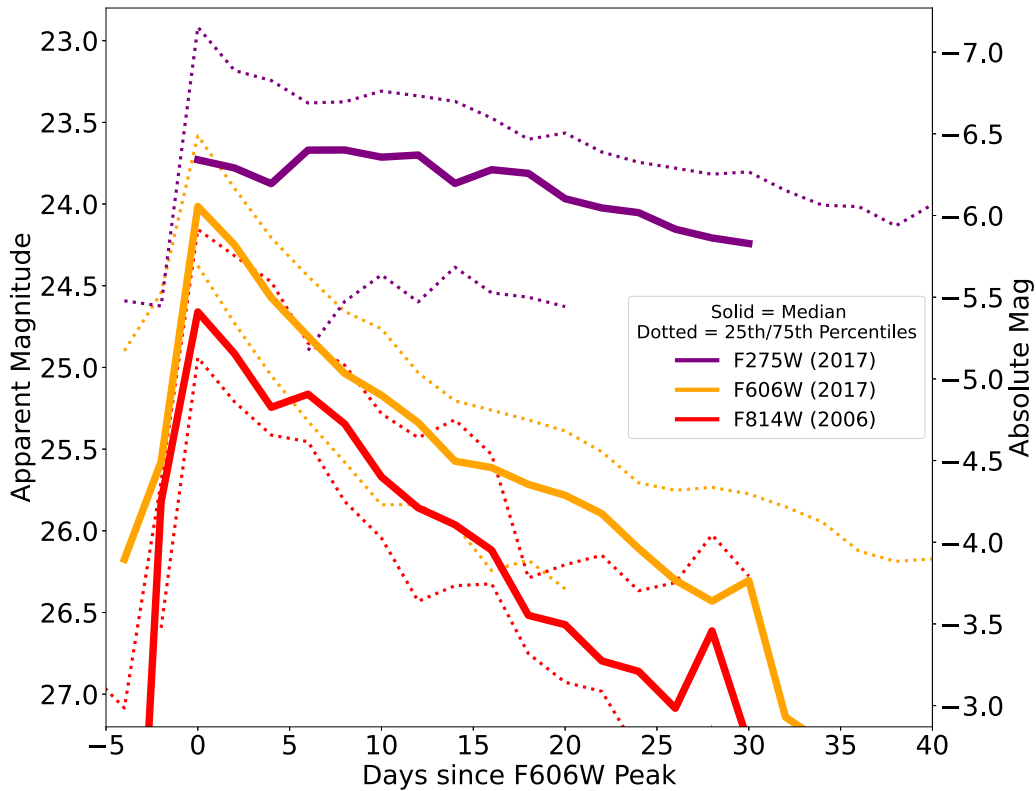


Figure 6. Median HST light curve of 77 M87 novae with observed peaks in F275W bandpass (solid purple) and F606W bandpass (solid orange), both based on 5 day cadence observations. Also shown are the median daily cadence light curves of 32 M87 novae in the F814W bandpass (red) of HST from Shara et al. (2016). For each band, the 25th and 75th percentiles of all light curves in that band are shown as dotted lines. The much slower declines of novae in the NUV are apparent, as is the later rise to the peak of many novae in the NUV.

estimate of the annual nova rate in the inner circle outside the inner 4".

An entire WFC3 frame covers only the central portion of M87, so there is no region in our images that we can use to empirically determine the sky background. Thus, we drizzled all of the F606W images in our study to create a master F606W image, and then used a least-squares fit to determine the sky background level and photometric zero-point needed to fit this drizzled image to the M87 ellipsoidal surface brightness photometry profile of Kormendy et al. (2009). We then measured the F606W magnitude of M87's light within the inner circle and outside 4" from the nucleus to be $m(\text{F606W}) = 9.45$. Kormendy et al. (2009)'s published a total M87 V magnitude is 8.30, so 34.5% of M87's light is contained in this region.

Applying this correction, we find that the annual nova rate within all of M87 is $R_{\text{nova}} = 352^{+37}_{-37} \text{ yr}^{-1}$.

This measurement of the overall nova rate is in very good agreement with the finding of Shara et al. (2016), whose shorter-duration, 72 day survey detected 32 *certain* and nine *possible* novae, yielded $R_{\text{nova}} = 363^{+33}_{-45} \text{ yr}^{-1}$. It is more than three times larger than the M87 nova rate of the much sparser-cadence, ground-based rate published by Shafter et al. (2000) ($91 \pm 34 \text{ yr}^{-1}$) and more than double the ground-based rate of Curtin et al. (2015) ($154^{+23}_{-19} \text{ yr}^{-1}$).

4.6. LSNR of M87

By adopting an M87 distance of $15.2 \pm 1.4 \text{ Mpc}$, Shafter et al. (2000) derived a K-band luminosity for M87 of

$39.8 \pm 8.2 \times 10^{10} L_{\odot, K}$. Correcting that luminosity to our adopted distance of $16.07 \pm 1.03 \text{ Mpc}$ (de Grijs & Bono 2019), and combining with this study's nova rate of $352^{+37}_{-37} \text{ yr}^{-1}$, we derive an M87 LSNR of $7.91^{+1.20}_{-1.20} \text{ yr}/10^{10} L_{\odot, K}$. This agrees closely with the value of Shara et al. (2016): $7.88^{+72}_{-98} \text{ yr}/10^{10} L_{\odot, K}$.

4.7. M87 Nova Rates—Two Recent Criticisms Answered

In response to the $363^{+33}_{-45} \text{ yr}^{-1}$ rate of Shara et al. (2016), Shafter et al. (2017) undertook an independent review of the HST dataset. They stated that...“Our results are in broad agreement with those of Shara et al., although we argue that the global nova rate in M87 remains uncertain, both due to the difficulty in identifying bona fide novae from incomplete light curves, and in extrapolating observations near the center of M87 to the entire galaxy. *We conclude that nova rates as low as ~ 200 per yr remain plausible.*” (Italics are ours.) We respond to these two suggestions as follows.

1. Almost all of the 94 novae reported in the present work are detected in both F606W and F275W images. (The few missing NUV light and color curves belong to novae which erupted late in our 9 month observing window. Our observations ended before these novae became detectable in the NUV). These transients' F275W–F606W colors are so blue (typically $m(\text{F275W}) - m(\text{F606W}) = -2$; see below) that we can preclude their being anything but classical novae, dwarf novae or active galactic nuclei (AGN) in eruption. Their spatial distribution follows the light of M87 so closely (see below) that they cannot

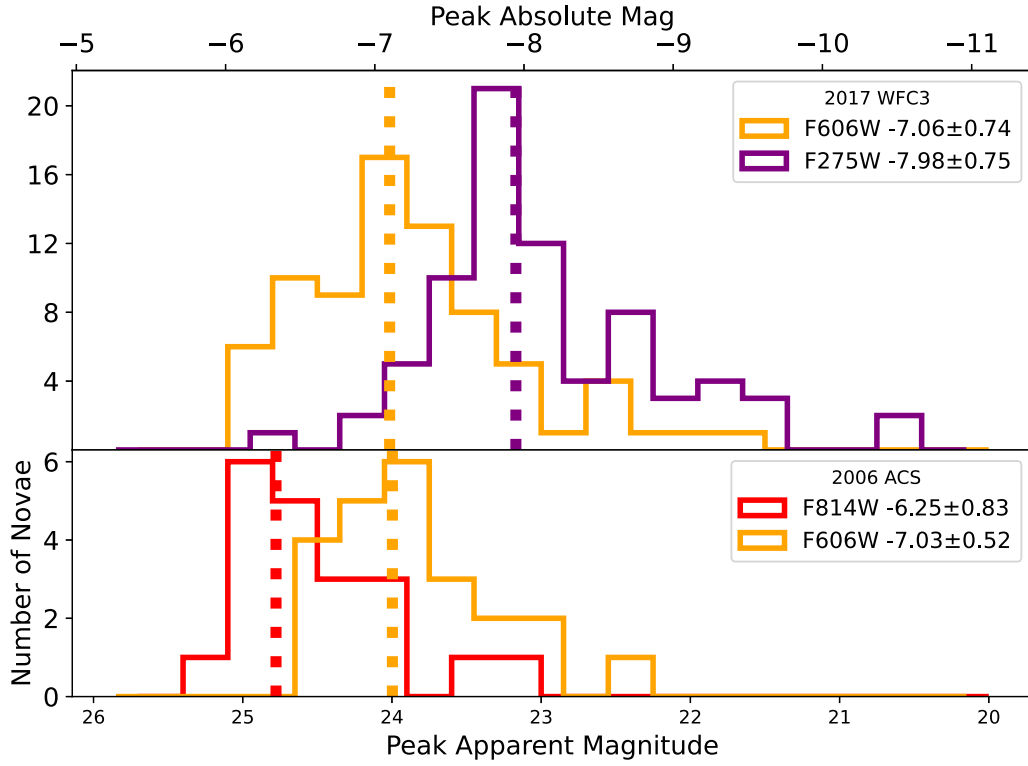


Figure 7. Top: the peak absolute magnitude distributions of 77 novae with observed peaks in 5 day cadence imagery of M87 in the F275W and F606W filters of HST, along with the median and standard deviations of the distribution. Novae are 0.9 mag more luminous at peak brightness in the NUV than in the visible. Bottom: a histogram of the peak F606W and F814W magnitudes from 1 day cadence imagery of M87 novae (Shara et al. 2016). Note that the median peak F606W magnitude from this 1 day cadence sample is almost identical to that of the 5 day cadence sample.

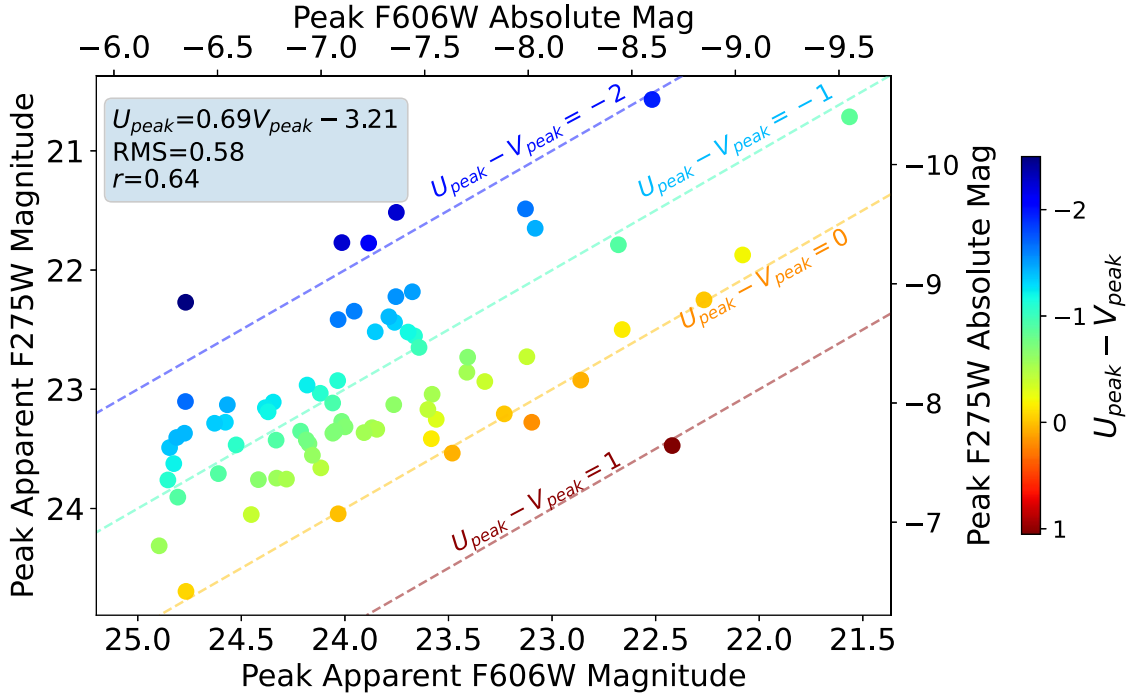


Figure 8. Peak F275W vs. peak F606W absolute magnitudes of the 77 novae with observed peaks in M87. The correlations are given in the figure legend.

be foreground dwarf novae or background AGN. They *can* only be erupting classical novae in M87.

2. Figure 3 of Curtin et al. (2015) demonstrated that novae follow the light of M87 with high fidelity (K-S test

statistic = 0.81) from $\sim 1'$ out to $10'$. In Figure 4 we plot the cumulative distributions of novae from this study, as well as the K-band and visible light in M87. The 94 novae we have detected follow the K-band light of M87 closely (K-S test

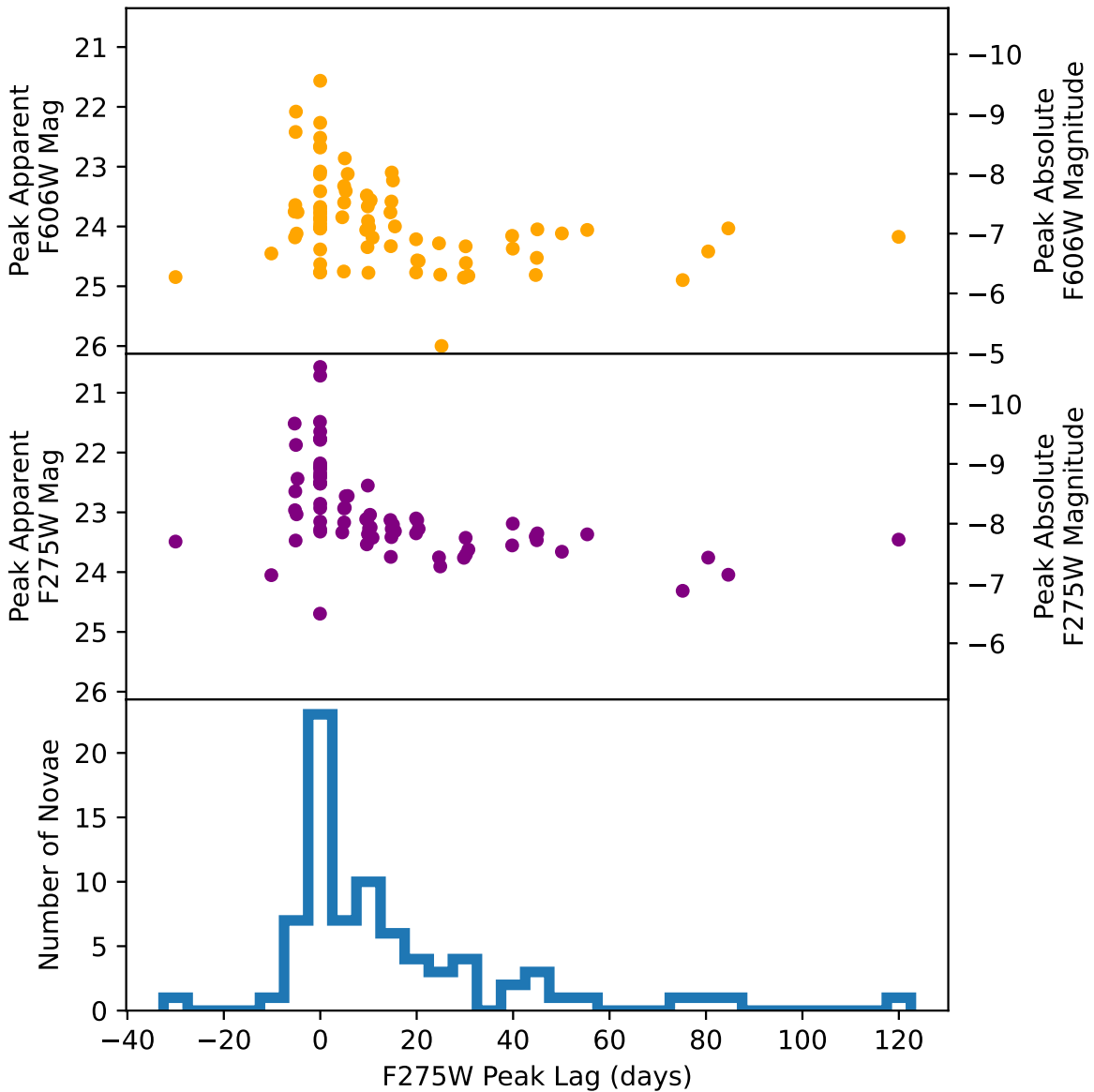


Figure 9. The number of days after the observed F606W peak that the F275W peak was observed plotted vs. peak F606W magnitude (top), vs. peak F275W magnitude (middle), and as a histogram (bottom). Data from the 77 novae whose peaks were observed are included in the plots.

statistic = 0.61). In particular, there is no discontinuity in the cumulative number of novae in the radial distance range $1' - 2'$ where our data overlaps those of Curtin et al. (2015). We conclude that extrapolating nova rates in the region encompassing the inner $\sim 1/3$ of M87's light to the whole galaxy is entirely justified by Figure 4 of this paper and Figure 3 of Curtin et al. (2015).

In summary, the extraordinarily blue F275W–F606W colors and spatial concentration around M87 of the transients reported in this paper uniquely identify these objects as erupting novae. The lack of any discontinuity in the cumulative radial distributions of M87 novae, which closely follow the K-band light in ground-based and space-based nova samples stretching from $4''$ to $10'$ from M87's nucleus, argues strongly that the HST-determined nova rate applies throughout M87.

We again emphasize that ground-based, sparsely sampled surveys hampered by the Moon, clouds, variable seeing, and irregular cadence, as well as simplistic simulations that model

novae instead of using real-world nova light curves, and which omit faint, fast novae, have all contributed to very significant underestimates of nova rates in galaxies.

An annual M87 nova rate of 300 or more seems inescapable. An LSNR of $\sim 7 - 10/\text{yr}/10^{10} L_{\odot, K}$ in *all* types of galaxies is indicated by the dense time coverage and HST data available in 2023.

5. Rapidly Recurring Novae

As the mass of a WD approaches the Chandrasekhar mass, the accreted envelope mass required to trigger a thermonuclear runaway decreases monotonically (see Figure 4 of Hillman et al. 2016). The simulations indicate that the time between nova eruptions can become as short as 45 days in the final years before a WD erupts as an SNIa. As of 2023, the most rapidly recurring nova known is located in M31 (Darnley et al. 2014). That nova, M31-2008-12a, erupts annually. One of the prime scientific drivers of the current

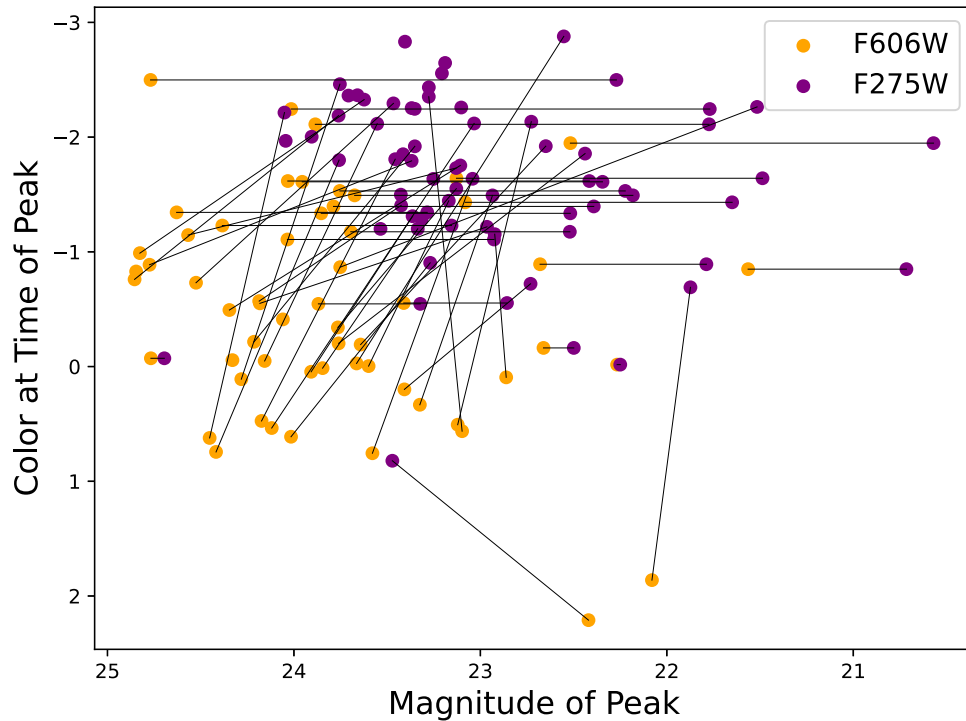


Figure 10. The $m(\text{F275W}) - m(\text{F606W})$ color at the time of the observed visible peak vs. the visible peak magnitude (orange) and the color at the time of the observed NUV peak vs. the NUV peak magnitude (purple). The two data points for each of the 55 novae that are observed in both bands at the time of both peaks are connected by a thin line. The horizontal lines represent novae whose observed visible and NUV peaks occurred at the same epoch. The most luminous novae (those with peak magnitudes < 23) achieve peak F275W and F606W brightnesses very close in time. Most (less luminous) novae exhibit fainter, redder F606W brightness peaks followed by more luminous, bluer F275W peaks.

study was to find or place strong limits on the number of even more rapidly recurring novae in M87.

The time baseline of the present survey is 260 days, so all novae recurring more frequently than every 130/86/65/52 days should have been seen to erupt at least twice/three times/four times/five times. None of the 94 novae detected in the current survey erupted more than once. We conclude that there are zero novae (in the inner $\sim 1/3$ of M87) recurring more frequently than once every 130 days. We defer modeling and a detailed discussion to place stringent limits on more infrequently recurring novae in M87 to a subsequent paper.

6. NUV, Visible, and NIR Light Behaviors of Novae

6.1. NUV and Visible Light Curves

At the top of Figure 5, we plot the F275W and F606W light curves of 94 M87 novae. Collectively, novae are seen to be ~ 0.9 mag more luminous in F275W than in F606W near maximum light. But over the course of the ensuing 2–3 weeks, the gap widens to ~ 2 mag. This is reflected in the bottom section of Figure 5, where novae are seen to be reddest at or shortly after maximum light, then become increasingly blue, reaching $m(\text{F275W}) - m(\text{F606W}) \sim -2 \pm 0.5$ about 3 weeks later. Similar striking color behavior is seen in Figure 8 of Shara et al. (2016), where the (F606W–F814W) colors of 32 M87 novae are reddest at and shortly after maximum light, then become approximately a magnitude bluer in the ensuing month.

6.2. NUV, Visible, and NIR Light Curves

In Figure 6, we plot the median F275W and F606W light curves of 77 M87 novae with observed peak brightnesses (from the present survey, with a 5 day cadence) and the F606W and F814W (near-infrared) light curves of 32 more novae (from the Shara et al. 2016 survey with 1 day cadence). This plot reinforces the facts that (1) novae are ~ 1 mag more luminous in NUV than visible light, (2) they are ~ 1 mag brighter in visible than near-infrared light, and (3) they fade much more slowly in NUV than in visible or NIR light.

6.3. Nova Peak Absolute Magnitude Distributions

In Figure 7, we plot the histograms of the observed peak absolute magnitudes of M87 novae. Novae peak at $M(\text{F275W}) = -8.0 \pm 0.8$ and at $M(\text{F606W}) = 7.1 \pm 0.7$ in the current, 5 day cadence dataset. They peak at $M(\text{606W}) = -7.0 \pm 0.5$ and at $M(\text{814W}) = -6.3 \pm 0.8$ in the Shara et al. (2016) 1 day cadence dataset. One day versus 5 day temporal sampling barely changes the detected absolute magnitudes of novae despite their being seen closer in time (on average) to the epoch of maximum light in the 1 day cadence data.

6.4. Correlations between Peak Magnitudes

In Figure 8, we plot the peak F275W magnitudes versus the peak F606W magnitudes for 77 M87 novae with both quantities observed. The strong correlation between the peak magnitudes (with $r = 0.64$) is apparent, and it would likely be even stronger if we had daily cadence data available. The data

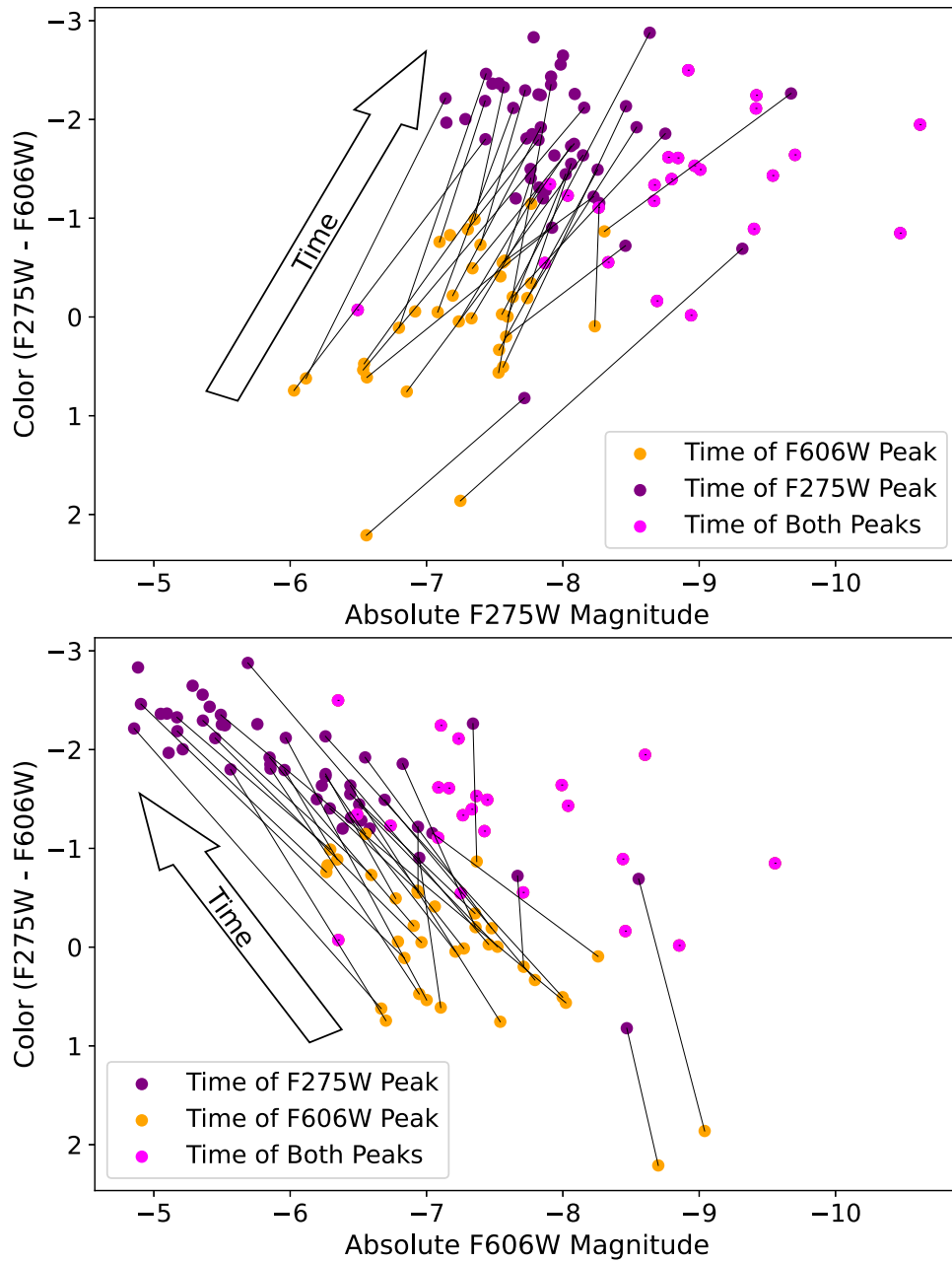


Figure 11. F275W–F606W colors of 55 novae vs. the absolute peak F275W and F606W magnitudes. The arrows labeled “Time” indicate directions of color and magnitude change between the F606W and F275W peak brightnesses. As in Figure 10, we see that the most luminous novae (those with peak absolute magnitudes < -8) achieve peak F275W and F606W brightnesses very close in time.

shown in Figures 5–8 will allow tests of the predicted multiwavelength light curves of novae of Hillman et al. (2014), but are beyond the scope of this paper.

6.5. Lag between NUV and Visible Peak Magnitudes

In Figure 9, we plot the number of days after the observed F606W peak that the F275W peak was observed versus peak F606W magnitude (top), versus the peak F275W magnitude (middle), and as a histogram (bottom). Just nine of 77 novae peak in F275W *before* peaking in F606W, and just by 5–10 days. In contrast, while the F275W maximum is typically observed 5–30 days after the F606W maximum, a few lags of 40–80 days are observed, as is one extreme event (nova 54) with a 120 day lag. As noted above, these lags are a direct test

of models of nova light curves (Hillman et al. 2014), and are beyond the scope of this paper.

6.6. Color–Magnitude Correlations

In Figure 10, we plot the F275W–F606W color at the time of the observed F606W peak versus the F606W peak magnitude (orange) and the same color at the time of the observed F275W peak versus the F275W peak magnitude (purple). The two data points for each of the 55 novae that are observed in both bands at the time both peaks are connected by a thin line. The horizontal lines represent novae whose observed visible and NUV peaks occurred at the same epoch.

In Figure 11, we plot the F275W–F606W colors of 55 novae versus the absolute peak F275W and F606W magnitudes. As in

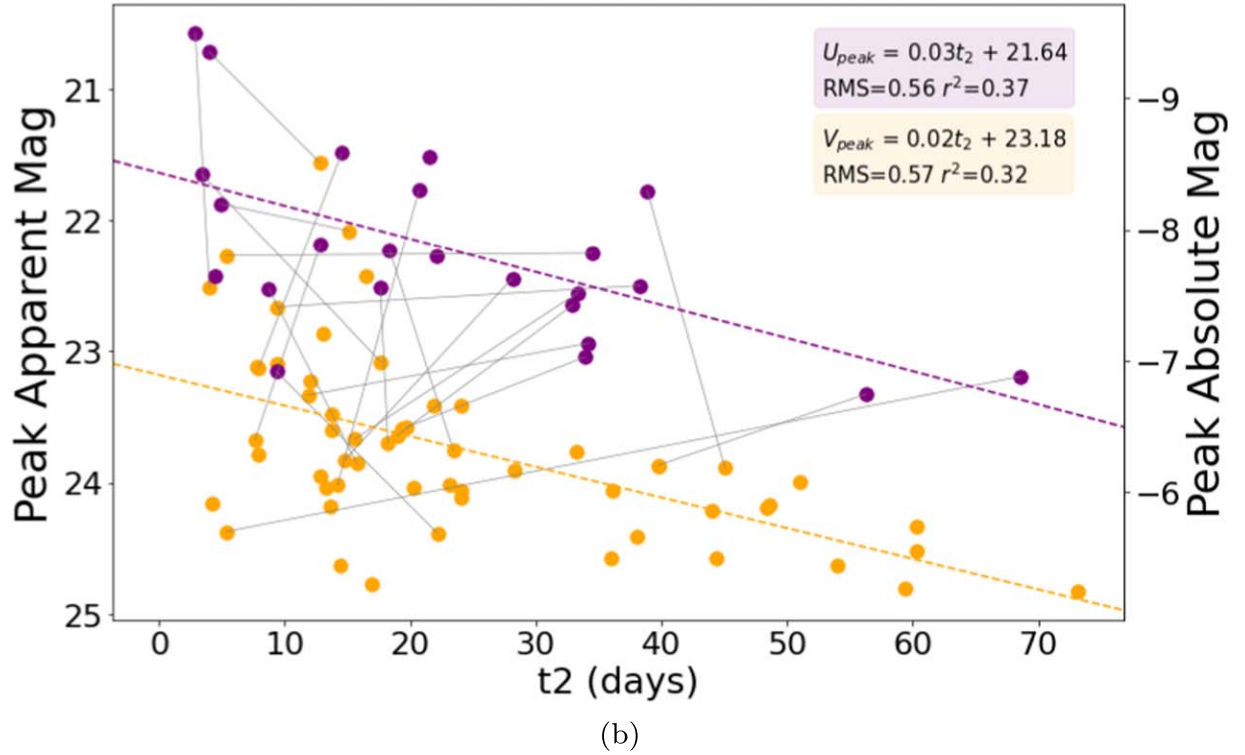
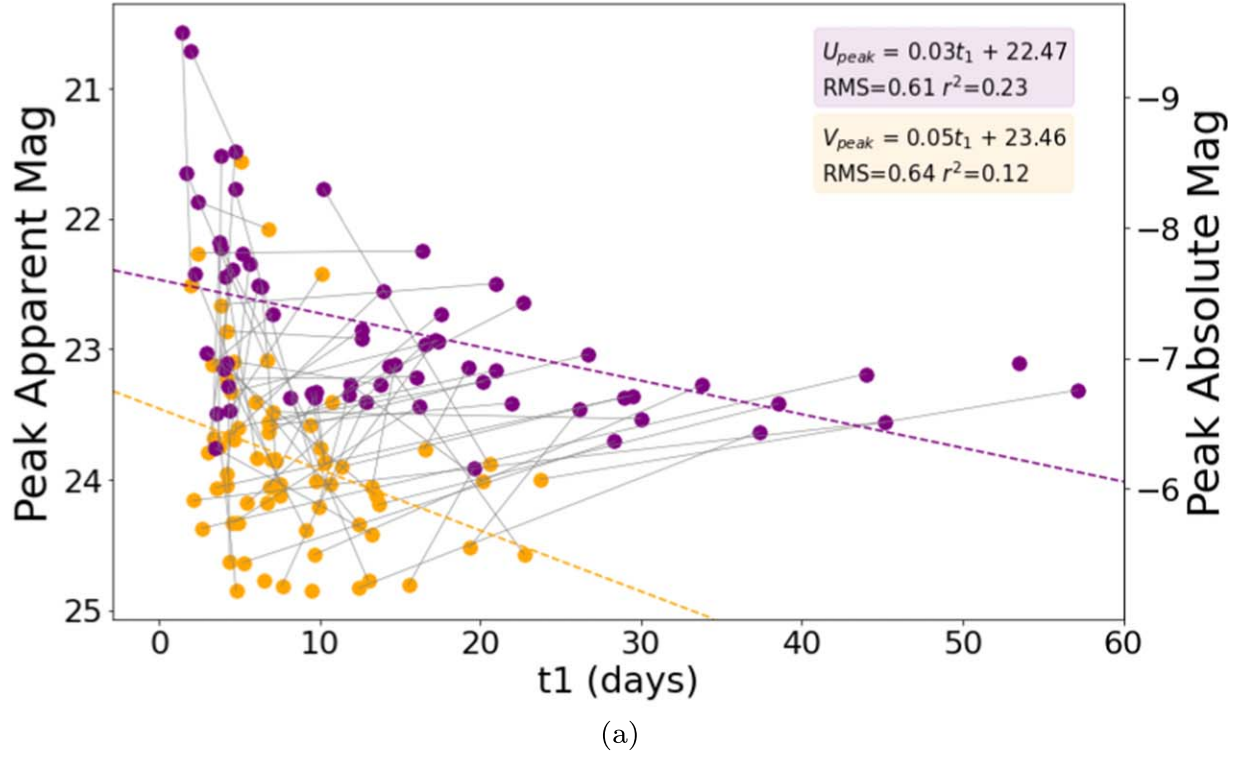


Figure 12. Top: F275W (violet) and F606W (yellow) peak magnitudes vs. t_1 decline time for novae with observed peak brightnesses. Each nova is plotted in both filters, and the pairs of points for each nova are connected by a thin line. Faint, fast novae are as prevalent in the F275W bandpass as in the F606W bandpass. Bottom: Same as above except F275W and F606W magnitudes vs. t_2 decline time.

Figure 10, we see that the most luminous novae (those with peak absolute magnitudes < -8) achieve peak F275W and F606W brightnesses very close in time. Most (less luminous) novae exhibit fainter, redder F606W brightness peaks followed by more luminous, bluer F275W peaks.

7. Absolute Magnitude versus Decline Time

Novae have been investigated as possible *standard candles* for over a century (Lundmark 1919; Mclaughlin 1945; Arp 1956; Shara 1981; Darnley et al. 2006; Della Valle & Izzo 2020; Schaefer 2022). If the eruptions of novae were

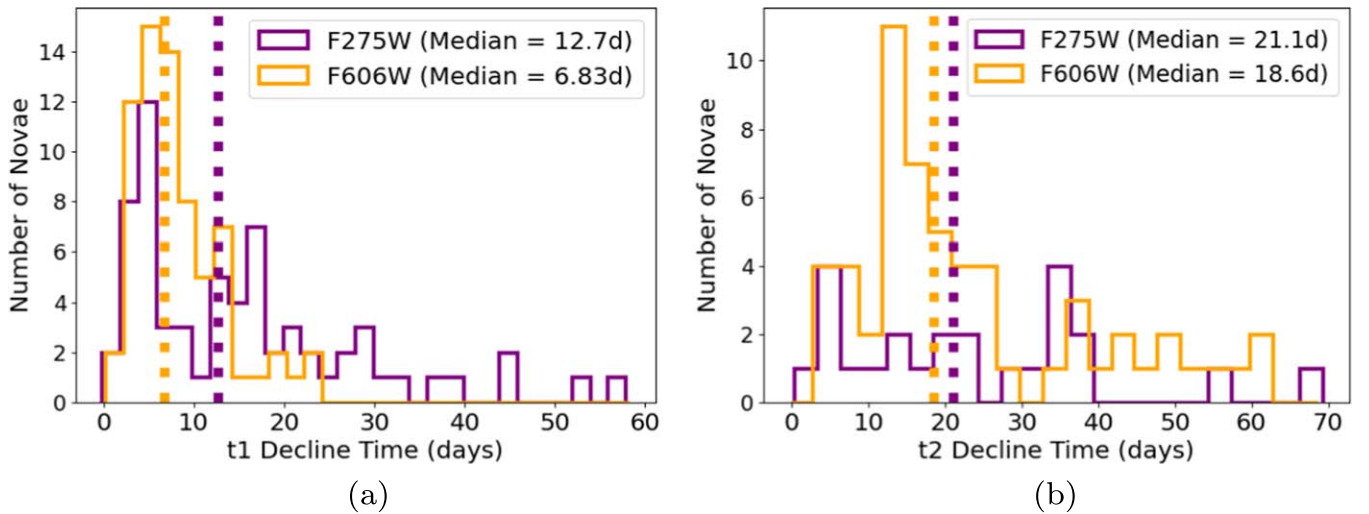


Figure 13. Left: histograms of the t_1 decline times in F275W and F606W of 77 novae in M87. The much slower t_1 declines in the NUV are apparent. Right: histograms of the t_2 decline times in F275W and F606W of 77 novae in M87. The declines in the NUV are slightly slower than in the visible, but much less so than for the t_1 decline times.

controlled by just one parameter—the underlying WD mass—then the absolute magnitudes of novae at peak brightness would all be strongly correlated with their rates of decline (Shara 1981), displaying an rms scatter of just ~ 0.5 mag. In fact, the critical masses of the thermonuclear-powered envelopes on WDs in nova binaries depend strongly on WD mass *and* mass accretion history, and to a lesser extent on the underlying WD luminosity (Yaron et al. 2005) and possibly the metallicity of accreted matter. It is thus no surprise that nova light curves are highly inhomogeneous. The definitive *snuffing out* of novae as standard candles came with Yaron et al. (2005)’s predictions of, and Kasliwal et al. (2011)’s observational discovery (in M31) of *faint, fast* novae. These objects are as common in the giant elliptical galaxy M87 (Shara et al. 2016) as in the giant spiral galaxy M31, strongly increasing the rms scatter in the peak visual absolute magnitude versus the decline time relationship of Galactic novae (Schaefer 2022, Figure 4). In the current era of precision cosmology, with Cepheid and tip-of-the-red giant branch distance indicators yielding $\sim 1\%$ accurate distances, the nova visual absolute magnitude— t_2 relationship is of little value as a distance indicator. Is the same true in the NUV?

In Figure 12, we plot the peak absolute magnitude versus t_1 and t_2 decline time relationships for 77 M87 novae with observed peak brightnesses. The rms scatter of each plot is close to 0.6 mag. Faint, fast novae are the strongest sources of scatter in both F275W and F606W bandpasses. This diagram demonstrates that, just as for F606W-detected novae, novae are not useful distance indicators in the F275W bandpass.

7.1. Decline Time Histograms

In Figure 13 we plot the histograms of one and two-magnitude decline times (t_1 and t_2 , respectively) of the 77 novae in the present sample with well-defined decline times. The mean t_1 of the F275W and F606W light curves of these novae are 12.7 and 6.83 days, respectively, while the corresponding t_2 are 21.1 and 18.6 days, respectively.

8. Correlations with Galactocentric Distance

In Figure 14, we plot the peak apparent magnitudes, t_1 decline times, and (F275W–F606W) color at peak brightness for 77 M87 novae versus radial distance from the nucleus of M87. The three plots are *scatter diagrams*, indicating that novae of all types, whether descendants of primordial binaries born in M87, or binaries captured during galaxy cannibalistic episodes, are thoroughly mixed in the galaxy.

9. Conclusions

We conducted a 9 month long, 5 day cadence NUV and visible-light HST survey for erupting M87 novae. The survey covered the inner $\sim 35\%$ of M87’s light. Simulations using *real-world* nova light curves showed the nova detection efficiency of the survey to be $\sim 75\%$. Taking a conservative 21% as the fraction of *faint, fast* novae in M87, we find the nova rate in M87 to be $352^{+37}_{-37} \text{ yr}^{-1}$, which is the value we adopt. (That rate would have increased to $\sim 380 \text{ yr}^{-1}$ if we had adopted a faint, fast nova fraction of $\sim 50\%$, as suggested by the M31 survey data of Kasliwal et al. 2011). The M87 LSNR is $7.91^{+1.20}_{-1.20} \text{ yr}/10^{10} L_{\odot, K}$. Both these rates are within 0.5 standard deviations of the rates previously derived in Shara et al. (2016), confirming their claim that previous ground-based surveys of M87—and by implication other ground-based surveys of all galaxies—are significantly incomplete. The radial distribution of novae closely followed M87’s light to within $\sim 4''$ of the galaxy’s nucleus. While theory predicts that novae can recur as often as every 45 days, we detect zero novae in the surveyed area erupting more frequently than once every 130 days. Novae are ~ 1 mag brighter in the NUV than in the visible at maximum light, and ~ 2 mag brighter in NUV than in near-IR light at maximum light. Novae are ~ 2 mag brighter in NUV light than in visible light ~ 3 weeks after peak brightness. The peak visible and NUV luminosities are strongly and positively correlated. Just nine of 77 novae achieved peak brightness in NUV light before visible light peak brightness was reached, with observed time lags between peak visible light and peak NUV light as long as 120 days. The most luminous novae (those with peak absolute

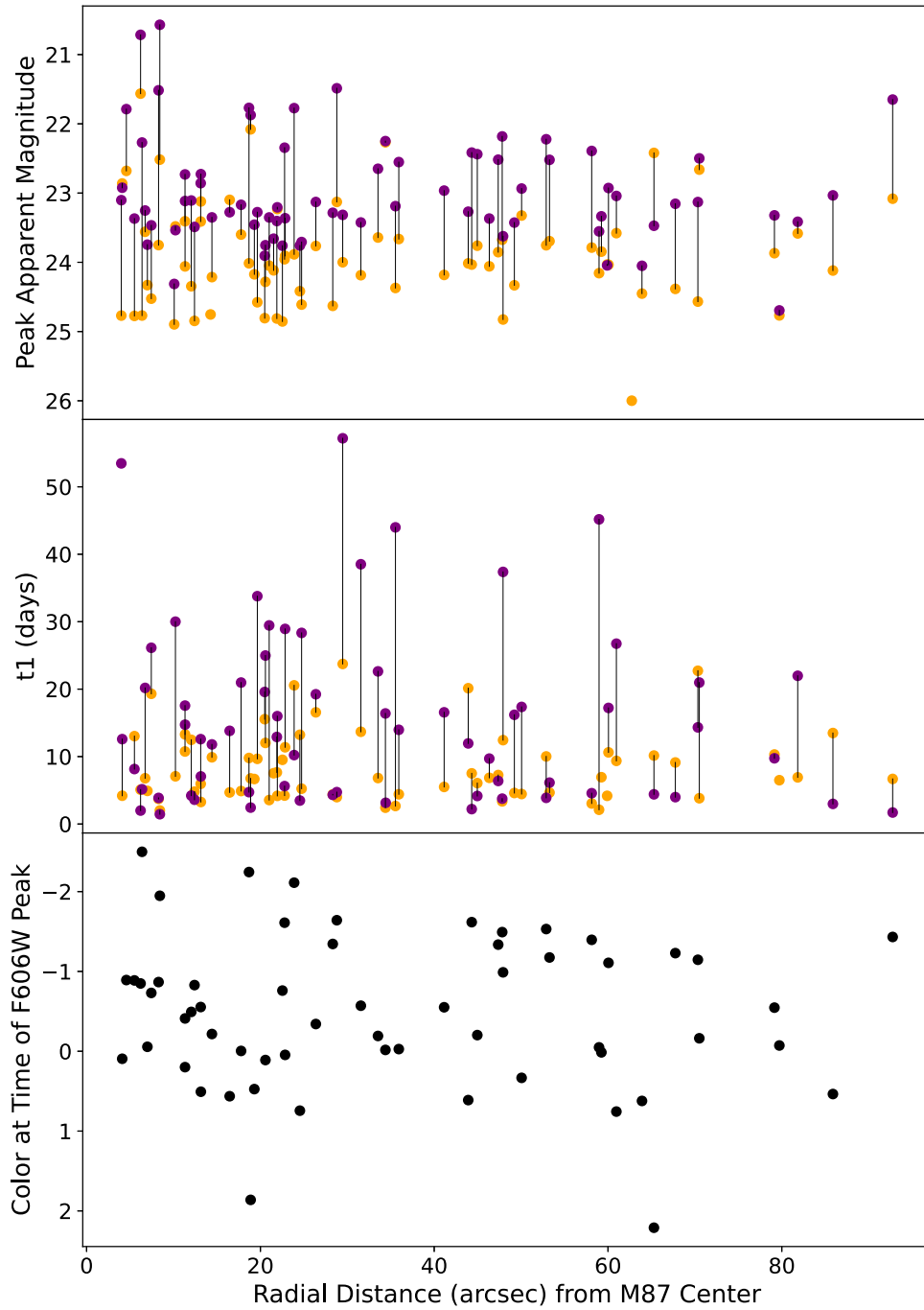


Figure 14. Peak apparent magnitude, t_1 decline time, and $(F_{275W}-F_{606W})$ color at peak brightness of the novae in M87 that had observed peaks. The lack of correlations means that novae of all luminosities, speed classes or origins are thoroughly mixed in the galaxy.

magnitudes < -8) achieve peak F275W and F606W brightnesses very close in time. Most (less luminous) novae exhibit fainter, redder F606W brightness peaks followed by more luminous, bluer F275W peaks.

Acknowledgments

This research is based on observations made with the NASA/ESA HST obtained from the Space Telescope Science Institute, which is operated by the Association of Universities for Research in Astronomy, Inc., under NASA contract NAS 5-26555. These observations are associated with programs

10543 (PI: Baltz) and 14618 (PI: Shara). The specific observations analyzed can be accessed via doi:[10.17909/natk-ks60](https://doi.org/10.17909/natk-ks60). Support to MAST for these data is provided by the NASA Office of Space Science via grant NAG5-7584 and by other grants and contracts. M.M.S. and R.H. were funded by NASA/STScI grant GO-14651. The paper also is based upon the work of R.H. supported by NASA under award No. 80GSFC21M0002. J.M. acknowledges the National Science Centre, Poland, grant OPUS 2017/27/B/ST9/01940. We thank the schedulers of HST for successfully obtaining the extremely regularly spaced 53 epochs of observations, which made the analyses presented here possible.

Facility: HST (WFC3 and ACS).

Software: CALWF3 (Dressel 2019), ASTRODRIZZLE (Avila et al. 2015), DAOFIND (Stetson 2011), PYRAF (Greenfield & White 2000).

Data Availability

All data described here are available on the STScI/MAST website: <https://mast.stsci.edu/search/ui/#/hst> and setting Proposal ID = 10543,14618.

Appendix Data

In Table 1, we list the HST image root names, observation dates, passbands, and exposure times collected for program GO-14618.

In Table 2, we list the positions, peak magnitudes, colors, and decline times of the 94 novae we detected in M87.

Table 3 lists the light-curve data for every nova: the epochs and corresponding date of detection, as well as the U (F275W) and V (F606W) magnitudes, (F275W–F606W) color, and their errors.

In Figure 15, we provide light and color curves and *postage stamp* images of each nova. The 94 novae are ordered by peak brightness in the F606W bandpass, where nova 1 is the most luminous and nova 94 is the least luminous.

The top-left section of each figure contains the F606W and F275W light curves of the nova. The bottom-left section contains the (F275W–F606W) color curve of the nova. The top-right section contains a series of $1''.1 \times 1''.3$ postage stamp F606W images of the nova in every epoch in which it was imaged by HST. North is up, east is left. The day of observation (0, 5, 10, 15, etc.) and the observed magnitude are just above each image. The bottom-right section is the same as the top-right section, except that it displays the F275W images of the same nova. The nova is marked with an orange (blue) tic mark on the day it reaches maximum light in F606W (F275W).

Table 1
HST GO-14618 WFC3 Observations of M87

Epoch #	Root Name	Obs Date (YYYY-MM-DD)	Band	Exp Time (s)	Epoch #	Root Name	Obs Date (YYYY-MM-DD)	Band	Exp Time (s)
1	id5o01rdq	2016-11-13	F275W	500.0	2	id5o02hmq	2016-11-18	F275W	520.0
1	id5o01req	2016-11-13	F275W	500.0	2	id5o02hoq	2016-11-18	F275W	520.0
1	id5o01rhq	2016-11-13	F275W	500.0	2	id5o02hqq	2016-11-18	F275W	520.0
1	id5o01rjq	2016-11-13	F606W	360.0	2	id5o02hsq	2016-11-18	F606W	360.0
1	id5o01rlq	2016-11-13	F606W	360.0	2	id5o02hxq	2016-11-18	F606W	360.0
3	id5o03diq	2016-11-23	F275W	520.0	4	id5o04avq	2016-11-28	F275W	520.0
3	id5o03djg	2016-11-23	F275W	520.0	4	id5o04axq	2016-11-28	F275W	520.0
3	id5o03dlq	2016-11-23	F275W	520.0	4	id5o04azq	2016-11-28	F275W	520.0
3	id5o03dnq	2016-11-23	F606W	360.0	4	id5o04b1q	2016-11-28	F606W	360.0
3	id5o03dpq	2016-11-23	F606W	360.0	4	id5o04b3q	2016-11-28	F606W	360.0
5	id5o05h4q	2016-12-03	F275W	500.0	6	id5o06v1q	2016-12-08	F275W	500.0
5	id5o05h5q	2016-12-03	F275W	500.0	6	id5o06v2q	2016-12-08	F275W	500.0
5	id5o05h7q	2016-12-03	F275W	500.0	6	id5o06v4q	2016-12-08	F275W	500.0
5	id5o05h9q	2016-12-03	F606W	360.0	6	id5o06v6q	2016-12-08	F606W	360.0
5	id5o05hbq	2016-12-03	F606W	360.0	6	id5o06v8q	2016-12-08	F606W	360.0
7	id5o07qiq	2016-12-13	F275W	500.0	8	id5o08p7q	2016-12-18	F275W	500.0
7	id5o07qjq	2016-12-13	F275W	500.0	8	id5o08p8q	2016-12-18	F275W	500.0
7	id5o07qlq	2016-12-13	F275W	500.0	8	id5o08paq	2016-12-18	F275W	500.0
7	id5o07qnq	2016-12-13	F606W	360.0	8	id5o08pcq	2016-12-18	F606W	360.0
7	id5o07ppq	2016-12-13	F606W	360.0	8	id5o08peq	2016-12-18	F606W	360.0
9	id5o09wkq	2016-12-23	F275W	500.0	10	id5o10nvq	2016-12-28	F275W	500.0
9	id5o09wlq	2016-12-23	F275W	500.0	10	id5o10o0q	2016-12-28	F275W	500.0
9	id5o09woq	2016-12-23	F275W	500.0	10	id5o10o2q	2016-12-28	F275W	500.0
9	id5o09wqq	2016-12-23	F606W	360.0	10	id5o10o5q	2016-12-28	F606W	360.0
9	id5o09wtq	2016-12-23	F606W	360.0	10	id5o10o8q	2016-12-28	F606W	360.0
11	id5o11acq	2017-01-02	F275W	500.0	12	id5o12hfg	2017-01-07	F275W	500.0
11	id5o11adq	2017-01-02	F275W	500.0	12	id5o12hgq	2017-01-07	F275W	500.0
11	id5o11afq	2017-01-02	F275W	500.0	12	id5o12hiq	2017-01-07	F275W	500.0
11	id5o11aiq	2017-01-02	F606W	360.0	12	id5o12hkq	2017-01-07	F606W	360.0
11	id5o11akq	2017-01-02	F606W	360.0	12	id5o12hmq	2017-01-07	F606W	360.0
13	id5o13z4q	2017-01-12	F275W	500.0	14	id5o14hsq	2017-01-17	F275W	520.0
13	id5o13z5q	2017-01-12	F275W	500.0	14	id5o14htq	2017-01-17	F275W	520.0
13	id5o13z7q	2017-01-12	F275W	500.0	14	id5o14ifq	2017-01-17	F275W	520.0
13	id5o13z9q	2017-01-12	F606W	360.0	14	id5o14ihq	2017-01-17	F606W	360.0
13	id5o13zbq	2017-01-12	F606W	360.0	14	id5o14ijq	2017-01-17	F606W	360.0
15	id5o15guq	2017-01-22	F275W	500.0	16	id5o16arq	2017-01-27	F275W	500.0
15	id5o15gvq	2017-01-22	F275W	500.0	16	id5o16asq	2017-01-27	F275W	500.0
15	id5o15gxq	2017-01-22	F275W	500.0	16	id5o16auq	2017-01-27	F275W	500.0
15	id5o15hlq	2017-01-22	F606W	360.0	16	id5o16awq	2017-01-27	F606W	360.0
15	id5o15hnq	2017-01-22	F606W	360.0	16	id5o16ayq	2017-01-27	F606W	360.0

Table 1
(Continued)

Epoch #	Root Name	Obs Date (YYYY-MM-DD)	Band	Exp Time (s)	Epoch #	Root Name	Obs Date (YYYY-MM-DD)	Band	Exp Time (s)
17	id5o17s5q	2017-02-01	F275W	500.0	18	id5o18dnq	2017-02-06	F275W	500.0
17	id5o17s6q	2017-02-01	F275W	500.0	18	id5o18doq	2017-02-06	F275W	500.0
17	id5o17s8q	2017-02-01	F275W	500.0	18	id5o18dqq	2017-02-06	F275W	500.0
17	id5o17saq	2017-02-01	F606W	360.0	18	id5o18dsq	2017-02-06	F606W	360.0
17	id5o17scq	2017-02-01	F606W	360.0	18	id5o18duq	2017-02-06	F606W	360.0
19	id5o19gvq	2017-02-11	F275W	500.0	20	id5o20tdq	2017-02-16	F275W	500.0
19	id5o19gwq	2017-02-11	F275W	500.0	20	id5o20teq	2017-02-16	F275W	500.0
19	id5o19gyq	2017-02-11	F275W	500.0	20	id5o20tqg	2017-02-16	F275W	500.0
19	id5o19hq	2017-02-11	F606W	360.0	20	id5o20tiq	2017-02-16	F606W	360.0
19	id5o19h2q	2017-02-11	F606W	360.0	20	id5o20tkq	2017-02-16	F606W	360.0
21	id5o21jvq	2017-02-21	F275W	500.0	22	id5o22kiq	2017-02-26	F275W	486.0
21	id5o21jwq	2017-02-21	F275W	500.0	22	id5o22kjq	2017-02-26	F275W	486.0
21	id5o21jyq	2017-02-21	F275W	500.0	22	id5o22klq	2017-02-26	F275W	486.0
21	id5o21k0q	2017-02-21	F606W	360.0	22	id5o22knq	2017-02-26	F606W	350.0
21	id5o21k2q	2017-02-21	F606W	360.0	22	id5o22kpq	2017-02-26	F606W	350.0
23	id5o23d8q	2017-03-03	F275W	486.0	24	id5o24o0q	2017-03-08	F275W	486.0
23	id5o23d9q	2017-03-03	F275W	486.0	24	id5o24o1q	2017-03-08	F275W	486.0
23	id5o23dbq	2017-03-03	F275W	486.0	24	id5o24o3q	2017-03-08	F275W	486.0
23	id5o23ddq	2017-03-03	F606W	350.0	24	id5o24o5q	2017-03-08	F606W	350.0
23	id5o23dfq	2017-03-03	F606W	350.0	24	id5o24o7q	2017-03-08	F606W	350.0
25	id5o25ehq	2017-03-13	F275W	472.0	26	id5o26fkq	2017-03-18	F275W	472.0
25	id5o25eiq	2017-03-13	F275W	472.0	26	id5o26flq	2017-03-18	F275W	472.0
25	id5o25ekq	2017-03-13	F275W	472.0	26	id5o26fnq	2017-03-18	F275W	472.0
25	id5o25emq	2017-03-13	F606W	349.0	26	id5o26fpq	2017-03-18	F606W	349.0
25	id5o25eoq	2017-03-14	F606W	349.0	26	id5o26frq	2017-03-18	F606W	349.0
27	id5o27q6q	2017-03-23	F275W	472.0	28	id5o28grq	2017-03-28	F275W	472.0
27	id5o27q7q	2017-03-23	F275W	472.0	28	id5o28gsq	2017-03-28	F275W	472.0
27	id5o27q9q	2017-03-23	F275W	472.0	28	id5o28guq	2017-03-28	F275W	472.0
27	id5o27qbq	2017-03-23	F606W	349.0	28	id5o28gwq	2017-03-28	F606W	349.0
27	id5o27qdq	2017-03-23	F606W	349.0	28	id5o28gyq	2017-03-28	F606W	349.0
29	id5o29d5q	2017-04-02	F275W	472.0	30	id5o30bnq	2017-04-07	F275W	472.0
29	id5o29d6q	2017-04-02	F275W	472.0	30	id5o30boq	2017-04-07	F275W	472.0
29	id5o29d8q	2017-04-02	F275W	472.0	30	id5o30bqq	2017-04-07	F275W	472.0
29	id5o29daq	2017-04-02	F606W	349.0	30	id5o30bsq	2017-04-07	F606W	349.0
29	id5o29dcq	2017-04-02	F606W	349.0	30	id5o30buq	2017-04-07	F606W	349.0
31	id5o31mpq	2017-04-12	F275W	486.0	32	id5o32boq	2017-04-17	F275W	500.0
31	id5o31mqq	2017-04-12	F275W	486.0	32	id5o32bpq	2017-04-17	F275W	500.0
31	id5o31msq	2017-04-12	F275W	486.0	32	id5o32brq	2017-04-17	F275W	500.0
31	id5o31muq	2017-04-12	F606W	350.0	32	id5o32btq	2017-04-17	F606W	360.0
31	id5o31mxq	2017-04-12	F606W	350.0	32	id5o32bvq	2017-04-17	F606W	360.0
33	id5o33izq	2017-04-22	F275W	500.0	34	id5o34tfq	2017-04-27	F275W	500.0
33	id5o33j0q	2017-04-22	F275W	500.0	34	id5o34tgq	2017-04-27	F275W	500.0
33	id5o33j2q	2017-04-22	F275W	500.0	34	id5o34tiq	2017-04-27	F275W	500.0
33	id5o33j4q	2017-04-22	F606W	360.0	34	id5o34tkq	2017-04-27	F606W	360.0
33	id5o33j6q	2017-04-22	F606W	360.0	34	id5o34tmq	2017-04-27	F606W	360.0
35	id5o35k1q	2017-05-02	F275W	520.0	36	id5o36i5q	2017-05-07	F275W	500.0
35	id5o35k2q	2017-05-02	F275W	520.0	36	id5o36i6q	2017-05-07	F275W	500.0
35	id5o35k4q	2017-05-02	F275W	520.0	36	id5o36i8q	2017-05-07	F275W	500.0
35	id5o35k6q	2017-05-02	F606W	360.0	36	id5o36iaq	2017-05-07	F606W	360.0
35	id5o35k8q	2017-05-02	F606W	360.0	36	id5o36icq	2017-05-07	F606W	360.0
37	id5o37ykq	2017-05-12	F275W	500.0	38	id5o38nfq	2017-05-17	F275W	500.0
37	id5o37ylq	2017-05-12	F275W	500.0	38	id5o38ngq	2017-05-17	F275W	500.0
37	id5o37ynq	2017-05-12	F275W	500.0	38	id5o38niq	2017-05-17	F275W	500.0
37	id5o37ypq	2017-05-12	F606W	360.0	38	id5o38nkq	2017-05-17	F606W	360.0
37	id5o37yrq	2017-05-12	F606W	360.0	38	id5o38nmq	2017-05-17	F606W	360.0
39	id5o39dkq	2017-05-22	F275W	500.0	40	id5o40fcq	2017-05-27	F275W	500.0
39	id5o39dmq	2017-05-22	F275W	500.0	40	id5o40fdq	2017-05-27	F275W	500.0
39	id5o39doq	2017-05-22	F275W	500.0	40	id5o40fgq	2017-05-27	F275W	500.0
39	id5o39dq	2017-05-22	F606W	360.0	40	id5o40fiq	2017-05-27	F606W	360.0
39	id5o39dsq	2017-05-22	F606W	360.0	40	id5o40fkq	2017-05-27	F606W	360.0
41	id5o41xtq	2017-06-01	F275W	500.0	42	id5o42lcq	2017-06-06	F275W	500.0
41	id5o41xuq	2017-06-01	F275W	500.0	42	id5o42ldq	2017-06-06	F275W	500.0

Table 1
(Continued)

Epoch #	Root Name	Obs Date (YYYY-MM-DD)	Band	Exp Time (s)	Epoch #	Root Name	Obs Date (YYYY-MM-DD)	Band	Exp Time (s)
41	id5o41xwq	2017-06-01	F275W	500.0	42	id5o42lfq	2017-06-06	F275W	500.0
41	id5o41xyq	2017-06-01	F606W	360.0	42	id5o42lhq	2017-06-06	F606W	360.0
41	id5o41y0q	2017-06-01	F606W	360.0	42	id5o42ljq	2017-06-06	F606W	360.0
43	id5o43m1q	2017-06-11	F275W	500.0	44	id5o44x0q	2017-06-16	F275W	500.0
43	id5o43m2q	2017-06-11	F275W	500.0	44	id5o44x1q	2017-06-16	F275W	500.0
43	id5o43m4q	2017-06-11	F275W	500.0	44	id5o44x3q	2017-06-16	F275W	500.0
43	id5o43m6q	2017-06-11	F606W	360.0	44	id5o44x5q	2017-06-16	F606W	360.0
43	id5o43m8q	2017-06-11	F606W	360.0	44	id5o44x7q	2017-06-16	F606W	360.0
45	id5o45bsq	2017-06-21	F275W	520.0	46	id5o46e5q	2017-06-26	F275W	520.0
45	id5o45btq	2017-06-21	F275W	520.0	46	id5o46e6q	2017-06-26	F275W	520.0
45	id5o45bvq	2017-06-21	F275W	520.0	46	id5o46e8q	2017-06-26	F275W	520.0
45	id5o45bxq	2017-06-21	F606W	360.0	46	id5o46eq	2017-06-26	F606W	360.0
45	id5o45bzq	2017-06-21	F606W	360.0	46	id5o46ecq	2017-06-26	F606W	360.0
47	id5o47z7q	2017-07-01	F275W	520.0	48	id5o48nmq	2017-07-06	F275W	500.0
47	id5o47z8q	2017-07-01	F275W	520.0	48	id5o48nnq	2017-07-06	F275W	500.0
47	id5o47zaq	2017-07-01	F275W	520.0	48	id5o48npq	2017-07-06	F275W	500.0
47	id5o47zcq	2017-07-01	F606W	360.0	48	id5o48nrq	2017-07-06	F606W	360.0
47	id5o47zeq	2017-07-01	F606W	360.0	48	id5o48ntq	2017-07-06	F606W	360.0
49	id5o49irq	2017-07-11	F275W	500.0	50	id5o50clq	2017-07-16	F275W	500.0
49	id5o49isq	2017-07-11	F275W	500.0	50	id5o50cmq	2017-07-16	F275W	500.0
49	id5o49iuq	2017-07-11	F275W	500.0	50	id5o50coq	2017-07-16	F275W	500.0
49	id5o49iwq	2017-07-11	F606W	360.0	50	id5o50cq	2017-07-16	F606W	360.0
49	id5o49iyq	2017-07-11	F606W	360.0	50	id5o50csq	2017-07-16	F606W	360.0
51	id5o51tpq	2017-07-21	F275W	500.0	52	id5o52m4q	2017-07-26	F275W	500.0
51	id5o51tqq	2017-07-21	F275W	500.0	52	id5o52m5q	2017-07-26	F275W	500.0
51	id5o51tsq	2017-07-21	F275W	500.0	52	id5o52m7q	2017-07-26	F275W	500.0
51	id5o51tuq	2017-07-21	F606W	360.0	52	id5o52m9q	2017-07-26	F606W	360.0
51	id5o51twq	2017-07-21	F606W	360.0	52	id5o52mbq	2017-07-26	F606W	360.0
53	id5o53cbq	2017-07-31	F275W	500.0	53	id5o53ccq	2017-07-31	F275W	500.0
53	id5o53ceq	2017-07-31	F275W	500.0	53	id5o53cgq	2017-07-31	F606W	360.0
53	id5o53cjg	2017-07-31	F606W	360.0					

Table 2
Positions, Peak Magnitudes, and Decline Times of M87 Novae

Nova #	Radial Distance (arcsec)	R.A. (HH:MM:SS.ss)	Decl. (HH:MM:SS.ss)	V_{peak} (mag)	U_{peak} (mag)	$(U - V)_{V_{\text{peak}}}$ (mag)	$(U - V)_{U_{\text{peak}}}$ (mag)	$U_{\text{peak}} - V_{\text{peak}}$ (mag)	$V t_1$ (days)	$U t_1$ (days)	$V t_2$ (days)	$U t_2$ (days)
1	6.21	12:30:49.40	+12:23:34.24	21.56	20.72	-0.85	-0.85	-0.85	5.09	1.99	12.86	3.99
2	18.88	12:30:48.41	+12:23:39.63	22.08	21.87	1.86	-0.69	-0.21	6.76	2.43	15.17	4.87
3	34.39	12:30:47.41	+12:23:45.75	22.27	22.25	-0.02	-0.02	-0.02	2.42	16.39	5.41	34.48
4	65.29	12:30:50.98	+12:24:29.20	22.42	23.47	2.21	0.82	1.05	10.15	4.40	16.49	...
5	8.43	12:30:49.13	+12:23:20.79	22.52	20.57	-1.95	-1.95	-1.95	2.00	1.45	4.01	2.91
6	70.51	12:30:48.66	+12:22:18.43	22.66	22.50	-0.16	-0.16	-0.16	3.82	20.98	9.35	38.33
7	4.58	12:30:49.13	+12:23:29.41	22.68	21.79	-0.89	-0.89	-0.89
8	4.10	12:30:49.15	+12:23:27.49	22.86	22.92	0.09	-1.15	0.06	4.20	12.58	13.04	...
9	92.76	12:30:45.95	+12:22:10.49	23.08	21.65	-1.43	-1.43	-1.43	6.69	1.70	17.69	3.41
10	16.46	12:30:48.46	+12:23:36.50	23.10	23.28	0.56	-2.35	0.18	4.68	13.82	9.35	...
11	13.15	12:30:50.30	+12:23:24.98	23.12	22.73	0.51	-2.13	-0.39	3.26	7.05	7.80	...
12	28.79	12:30:51.27	+12:23:18.12	23.13	21.49	-1.64	-1.64	-1.64	3.99	4.73	7.92	14.55
13	21.95	12:30:48.03	+12:23:20.05	23.23	23.21	...	-2.56	-0.02	4.17	15.99	11.98	...
14	50.06	12:30:46.09	+12:23:39.35	23.32	22.93	0.33	-1.49	-0.39	4.45	17.36	11.88	34.21
15	11.33	12:30:48.69	+12:23:24.50	23.41	22.73	0.20	-0.72	-0.68	10.75	17.56	21.86	...
16	13.13	12:30:48.61	+12:23:33.49	23.41	22.86	-0.55	-0.55	-0.55	5.96	12.58	24.11	...
17	10.22	12:30:50.00	+12:23:33.73	23.48	23.54	...	-1.20	0.05	7.07	30.00	13.79	...
18	6.74	12:30:49.74	+12:23:23.18	23.56	23.25	...	-1.64	-0.31	6.79	20.18
19	60.96	12:30:50.06	+12:24:28.29	23.58	23.04	0.76	-1.64	-0.54	9.36	26.74	19.72	33.95
20	81.83	12:30:44.28	+12:22:56.30	23.58	23.41	...	-1.85	-0.17	6.92	21.98	19.34	...
21	17.78	12:30:49.31	+12:23:45.75	23.60	23.17	-0.00	-1.44	-0.43	4.89	20.98	13.70	...
22	33.53	12:30:47.46	+12:23:10.79	23.64	22.65	-0.19	-1.92	-0.99	6.82	22.63	18.97	32.93
23	35.93	12:30:48.25	+12:23:59.58	23.66	22.55	-0.03	-2.88	-1.11	4.41	13.97	15.59	33.39
24	47.83	12:30:49.95	+12:22:40.84	23.67	22.18	-1.49	-1.49	-1.49	3.36	3.76	7.64	12.85
25	53.27	12:30:48.31	+12:22:37.35	23.70	22.52	-1.17	-1.17	-1.17	4.66	6.14	18.26	17.66
26	8.28	12:30:48.86	+12:23:26.76	23.75	21.52	-0.87	-2.26	-2.24	3.72	3.87	...	21.59
27	52.89	12:30:51.42	+12:22:44.01	23.75	22.22	-1.53	-1.53	-1.53	10.02	3.88	23.46	18.39
28	26.38	12:30:47.85	+12:23:40.82	23.76	23.13	-0.34	-1.55	-0.64	16.56	19.24	33.19	...
29	58.12	12:30:50.42	+12:22:31.79	23.79	22.39	-1.40	-1.40	-1.40	3.05	4.57	7.89	...
30	44.96	12:30:46.42	+12:23:37.24	23.76	22.44	-0.20	-1.86	-1.32	6.06	4.16	14.77	28.16
31	59.24	12:30:53.30	+12:23:11.02	23.85	23.34	0.01	-1.20	-0.51	6.94
32	47.36	12:30:48.95	+12:22:41.19	23.85	22.52	-1.34	-1.34	-1.34	7.26	6.39	15.77	8.72
33	23.88	12:30:48.05	+12:23:40.96	23.89	21.77	-2.11	-2.11	-2.11	20.56	10.22	45.06	38.89
34	22.84	12:30:50.88	+12:23:36.30	23.91	23.36	0.05	-1.31	-0.54	11.38	28.93	28.28	...
35	22.78	12:30:50.88	+12:23:19.94	23.96	22.35	-1.61	-1.61	-1.61	4.22	5.62	12.84	...
36	29.47	12:30:47.42	+12:23:30.08	24.00	23.32	...	-1.28	-0.68	23.73	57.20	51.03	...
37	18.69	12:30:50.57	+12:23:36.34	24.01	21.77	-2.24	-2.24	-2.24	9.79	4.73	14.23	20.72
38	43.92	12:30:51.82	+12:23:54.35	24.02	23.27	0.61	-0.90	-0.75	20.14	11.95	23.18	...
39	44.32	12:30:46.47	+12:23:18.71	24.03	22.42	-1.62	-1.62	-1.62	7.51	2.21	...	4.42
40	60.06	12:30:51.21	+12:22:33.99	24.03	22.93	-1.11	-1.11	-1.11	10.62	17.21	20.26	...
41	85.88	12:30:52.36	+12:22:13.73	24.12	23.03	0.54	-2.12	-1.09	13.49	2.98
42	7.45	12:30:49.76	+12:23:22.44	24.53	23.47	-0.73	-2.29	-1.06	19.31	26.13	60.32	...
43	3.99	12:30:49.20	+12:23:25.81	24.77	23.10	...	-2.26	-1.67	...	53.48
44	5.50	12:30:49.62	+12:23:23.33	24.77	23.37	-0.89	-1.79	-1.41	13.03	8.15
45	80.58	12:30:46.41	+12:24:35.41	<25.94	<23.96
46	16.56	12:30:50.12	+12:23:14.98	<23.74	<24.28
47	79.15	12:30:44.04	+12:23:34.95	23.87	23.32	-0.55	-0.55	-0.55	10.31	9.75	39.75	56.31
48	59.90	12:30:48.99	+12:24:27.61	24.03	24.04	...	-1.97	0.01	4.18	...	13.26	...
49	11.33	12:30:49.08	+12:23:17.92	24.06	23.12	-0.41	...	-0.94	13.29	14.73
50	46.34	12:30:50.61	+12:22:45.12	24.06	23.37	...	-2.25	-0.69	6.85	9.70	24.07	...
51	21.01	12:30:50.41	+12:23:43.36	24.05	23.35	...	-2.25	-0.70	3.55	29.45	36.11	...
52	21.52	12:30:50.25	+12:23:45.81	24.12	23.66	...	-2.37	-0.46	7.53	...	24.09	...
53	58.97	12:30:53.04	+12:23:21.15	24.16	23.55	-0.05	-2.12	-0.60	2.11	45.17	4.23	...

Table 2
(Continued)

Nova #	Radial Distance (arcsec)	R.A. (HH:MM:SS.ss)	Decl. (HH:MM:SS.ss)	V_{peak} (mag)	U_{peak} (mag)	$(U - V)_{V_{\text{peak}}}$ (mag)	$(U - V)_{U_{\text{peak}}}$ (mag)	$U_{\text{peak}} - V_{\text{peak}}$ (mag)	$V t_1$ (days)	$U t_1$ (days)	$V t_2$ (days)	$U t_2$ (days)
54	19.30	12:30:49.01	+12:23:46.38	24.17	23.46	0.47	-1.81	-0.72	6.67	...	48.61	...
55	41.14	12:30:47.32	+12:23:0.73	24.18	22.96	-0.55	-1.22	-1.22	5.50	16.56	13.62	...
56	31.56	12:30:51.58	+12:23:27.76	24.19	23.42	-0.57	-1.40	-0.76	13.68	38.52	48.35	...
57	14.42	12:30:49.07	+12:23:41.52	24.21	23.35	-0.22	-1.92	-0.86	9.89	11.80	44.07	...
58	7.00	12:30:49.29	+12:23:34.76	24.33	23.75	-0.06	...	-0.58	4.91
59	49.22	12:30:51.53	+12:24:6.39	24.33	23.43	...	-1.50	-0.91	4.60	16.20	60.33	...
60	12.05	12:30:48.60	+12:23:29.01	24.35	23.11	-0.49	-1.75	-1.24	12.49	4.21
61	35.54	12:30:50.14	+12:24:1.98	24.37	23.19	...	-2.65	-1.18	2.67	43.99	5.34	68.59
62	24.54	12:30:47.93	+12:23:39.16	24.42	23.76	0.74	-1.80	-0.66	13.23	3.48	38.06	...
63	5.59	12:30:49.64	+12:23:32.67	<25.08	<23.62
64	20.58	12:30:50.70	+12:23:19.59	<24.28	<23.75	12.03	24.98	24.08	...
65	67.75	12:30:48.98	+12:22:20.60	24.38	23.15	-1.23	-1.23	-1.23	9.12	3.98	22.18	9.34
66	63.91	12:30:45.06	+12:23:26.44	24.45	24.05	0.62	-2.21	-0.40
67	70.34	12:30:49.65	+12:22:17.78	24.57	23.13	-1.15	-1.73	-1.44	22.72	14.33	35.95	...
68	19.65	12:30:48.17	+12:23:21.16	24.58	23.28	...	-2.43	-1.30	9.66	33.78	44.33	...
69	28.33	12:30:50.99	+12:23:44.74	24.63	23.29	-1.34	-1.34	-1.34	4.39	4.32	14.41	...
70	24.74	12:30:47.94	+12:23:39.94	24.61	23.71	...	-2.36	-0.90	5.24	28.34	53.97	...
71	14.27	12:30:48.45	+12:23:26.72	24.75
72	79.72	12:30:44.20	+12:23:5.63	24.77	24.69	-0.07	-0.07	-0.07	6.50	...	16.97	...
73	20.50	12:30:50.82	+12:23:29.78	24.81	23.90	...	-2.00	-0.90	15.54	19.58	59.35	...
74	21.89	12:30:50.92	+12:23:27.65	24.81	23.40	...	-2.83	-1.41	7.66	12.91
75	47.92	12:30:50.14	+12:22:41.27	24.83	23.62	-0.99	-2.33	-1.20	12.44	37.38	73.18	...
76	12.42	12:30:49.38	+12:23:40.44	24.85	23.49	-0.83	...	-1.36	4.80	3.60
77	22.53	12:30:49.06	+12:23:6.15	24.85	23.76	-0.76	-2.19	-1.09	9.52
78	10.08	12:30:50.09	+12:23:30.32	24.90	24.31	-0.58
79	25.35	12:30:49.57	+12:23:2.79	<25.04	<23.75
80	34.42	12:30:51.73	+12:23:21.49	<24.87	<23.54	3.15
81	43.78	12:30:52.38	+12:23:21.73	<24.85	<23.81
82	35.78	12:30:50.23	+12:24:1.82	<25.16	<23.13
83	40.49	12:30:51.25	+12:23:58.47	<24.76	<24.00
84	42.39	12:30:47.17	+12:23:1.46	<24.98	<23.87
85	40.57	12:30:48.54	+12:24:6.49	<25.31	<23.33
86	21.77	12:30:50.01	+12:23:8.02	<25.45	<23.77
87	20.54	12:30:50.14	+12:23:45.73	<25.21	<23.04
88	20.51	12:30:48.02	+12:23:28.35	<25.27	<23.39
89	60.99	12:30:45.94	+12:24:1.35	<25.91	<24.34
90	49.09	12:30:48.85	+12:24:16.42	<25.47	<24.18
91	62.73	12:30:46.19	+12:24:9.22	26.00
92	99.38	12:30:43.70	+12:24:21.31	<25.86	<23.68
93	24.64	12:30:50.93	+12:23:17.25	<24.14	<23.08
94	6.38	12:30:49.00	+12:23:29.70	24.77	22.27	-2.50	-2.50	-2.50	...	5.15	...	22.10

(This table is available in machine-readable form.)

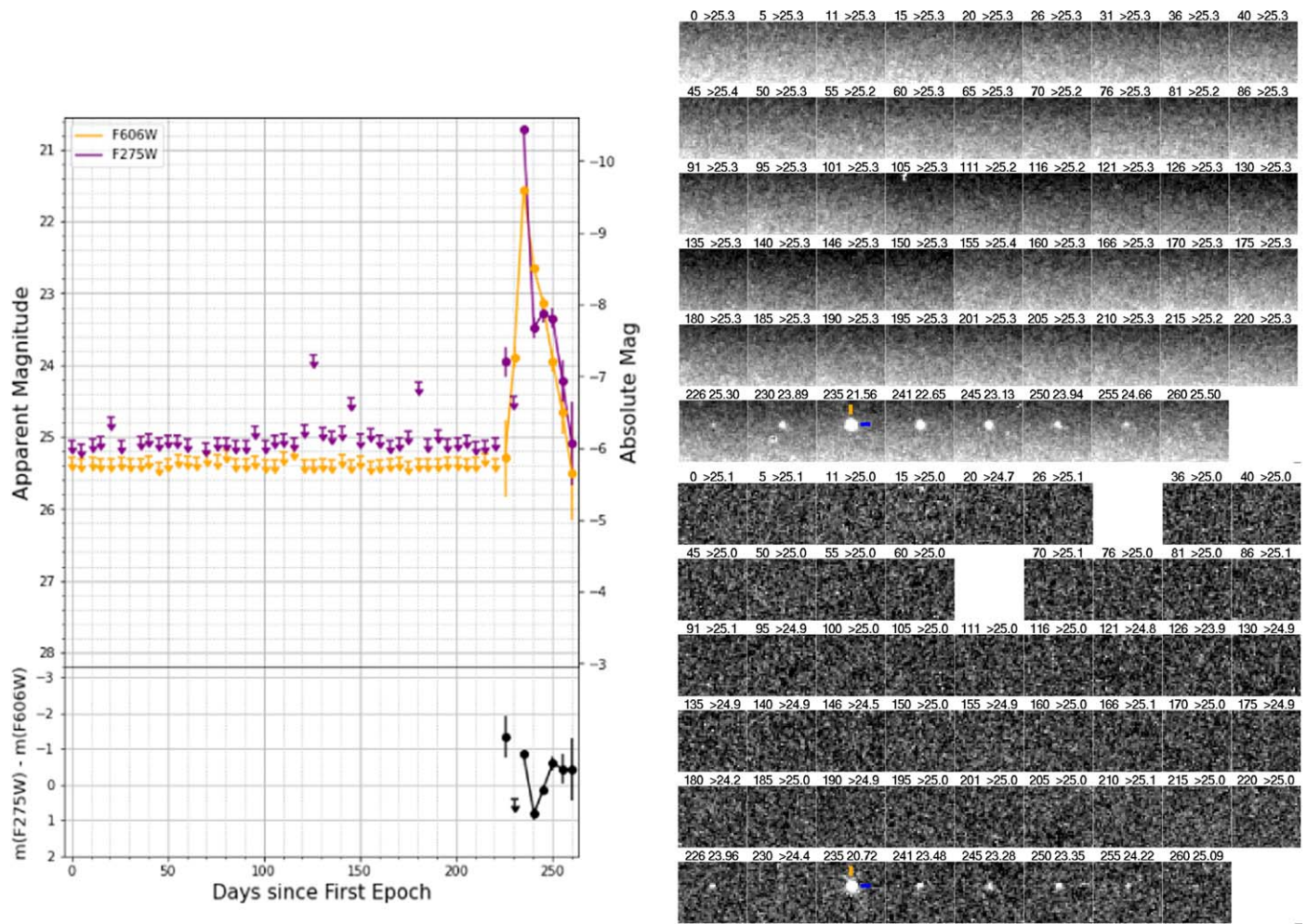


Figure 15. Nova 1. See the [Appendix](#) for a description of this figure.
(The complete figure set (94 images) is available.)














Table 3
M87 Nova Light-curve Data

Epoch #	Days Since First Ep	Days Since F606W Peak	Days Since F275W Peak	V (mag)	V_{err} (mag)	U (mag)	U_{err} (mag)	$(U - V)$ (mag)	$(U - V)_{\text{err}}$ (mag)
M87 Nova 1									
44	215.26	-19.87	-19.87	>25.23	...	>25.05
45	220.48	-14.65	-14.65	>25.31	...	>25.02
46	225.58	-9.55	-9.55	25.30	0.53	23.96	0.21	-1.34	0.57
47	230.23	-4.90	-4.90	23.89	0.15	>24.43
48	235.13	0.00	0.00	21.56	0.02	20.72	0.02	-0.85	0.03
49	240.66	5.55	5.51	22.65	0.05	23.48	0.14	0.82	0.15
50	245.26	10.13	10.13	23.13	0.08	23.28	0.13	0.15	0.15
51	250.36	15.23	15.23	23.94	0.16	23.35	0.13	-0.60	0.21
52	255.39	20.26	20.26	24.66	0.30	24.22	0.29	-0.44	0.42
53	260.29	25.17	25.17	25.50	0.65	25.09	0.58	-0.41	0.87

Note. Table 3 is published in its entirety online, with full data for all 53 epochs for all 94 novae, in the machine-readable format. A portion is shown here for guidance regarding its form and content. The precise time of the “First Ep” is MJD 57705.0605.

(This table is available in its entirety in machine-readable form.)

ORCID iDs

Michael M. Shara  <https://orcid.org/0000-0003-0155-2539>
 Alec M. Lessing  <https://orcid.org/0000-0001-6714-2706>
 Rebekah Hounsell  <https://orcid.org/0000-0002-0476-4206>
 Shifra Mandel  <https://orcid.org/0000-0002-6126-7409>
 David Zurek  <https://orcid.org/0009-0008-4599-2935>
 Matthew J. Darnley  <https://orcid.org/0000-0003-0156-3377>
 Or Graur  <https://orcid.org/0000-0002-4391-6137>
 Yael Hillman  <https://orcid.org/0000-0002-0023-0485>
 Eileen T. Meyer  <https://orcid.org/0000-0002-7676-9962>
 Joanna Mikolajewska  <https://orcid.org/0000-0003-3457-0020>
 James D. Neill  <https://orcid.org/0000-0002-0466-1119>
 Dina Prialnik  <https://orcid.org/0000-0002-6317-4839>
 William Sparks  <https://orcid.org/0000-0002-9011-6829>

References

- Arp, H. C. 1956, *AJ*, **61**, 15
- Avila, R. J., Hack, W., Cara, M., et al. 2015, in ASP Conf. Ser. 495, *Astronomical Data Analysis Software and Systems XXIV (ADASS XXIV)*, ed. A. R. Taylor & E. Rosolowsky (San Francisco, CA: ASP), 281
- Bertin, E., & Arnouts, S. 1996, *A&AS*, **117**, 393
- Cao, Y., Kasliwal, M. M., Neill, J. D., et al. 2012, *ApJ*, **752**, 133
- Cardelli, J. A., Clayton, G. C., & Mathis, J. S. 1989, *ApJ*, **345**, 245
- Chen, H.-L., Woods, T. E., Yungelson, L. R., Gilfanov, M., & Han, Z. 2016, *MNRAS*, **458**, 2916
- Claeys, J. S. W., Pols, O. R., Izzard, R. G., Vink, J., & Verbunt, F. W. M. 2014, *A&A*, **563**, A83
- Curtin, C., Shafter, A. W., Pritchett, C. J., et al. 2015, *ApJ*, **811**, 34
- Darnley, M. J., Bode, M. F., Kerins, E., et al. 2006, *MNRAS*, **369**, 257
- Darnley, M. J., Williams, S. C., Bode, M. F., et al. 2014, *A&A*, **563**, L9
- de Grijs, R., & Bono, G. 2019, *ApJS*, **246**, 3
- De, K., Kasliwal, M. M., Hankins, M. J., et al. 2021, *ApJ*, **912**, 19
- Della Valle, M., & Izzo, L. 2020, *A&ARv*, **28**, 3
- Dressel, L. 2019, *WFC3 Instrument Handbook for Cycle 27*, Vol. 11 (Baltimore, MD: STScI)
- Gallagher, J. S. I., & Code, A. D. 1974, *ApJ*, **189**, 303
- Greenfield, P., & White, R. L. 2000, in ASP Conf. Ser. 216, *Astronomical Data Analysis Software and Systems IX*, ed. N. Manset, C. Veillet, & D. Crabtree (San Francisco, CA: ASP), 59
- Harris, W. E. 2009, *ApJ*, **703**, 939
- Harris, W. E., & Petrie, P. L. 1978, *ApJ*, **223**, 88
- Hillman, Y. 2021, *MNRAS*, **505**, 3260
- Hillman, Y., Prialnik, D., Kovetz, A., & Shara, M. M. 2015, *MNRAS*, **446**, 1924
- Hillman, Y., Prialnik, D., Kovetz, A., & Shara, M. M. 2016, *ApJ*, **819**, 168
- Hillman, Y., Prialnik, D., Kovetz, A., Shara, M. M., & Neill, J. D. 2014, *MNRAS*, **437**, 1962
- Hillman, Y., Shara, M. M., Prialnik, D., & Kovetz, A. 2020, *NatAs*, **4**, 886
- Jha, S. W., Maguire, K., & Sullivan, M. 2019, *NatAs*, **3**, 706
- Kasliwal, M. M., Cenko, S. B., Kulkarni, S. R., et al. 2011, *ApJ*, **735**, 94
- Kawash, A., Chomiuk, L., Rodriguez, J. A., et al. 2021, *ApJ*, **922**, 25
- Kormendy, J., Fisher, D. B., Cornell, M. E., & Bender, R. 2009, *ApJS*, **182**, 216
- Liu, Z.-W., Röpke, F. K., & Han, Z. 2023, *RAA*, **23**, 082001
- Lundmark, K. 1919, *AN*, **209**, 369
- Madrid, J. P., Sparks, W. B., Ferguson, H. C., Livio, M., & Macchetto, D. 2007, *ApJL*, **654**, L41
- Mandel, S., Shara, M. M., Zurek, D., Conroy, C., & van Dokkum, P. 2023, *MNRAS*, **518**, 5279
- Maoz, D., Mannucci, F., & Nelemans, G. 2014, *ARA&A*, **52**, 107
- Matteucci, F., Renda, A., Pipino, A., & Della Valle, M. 2003, *A&A*, **405**, 23
- McLaughlin, D. B. 1945, *PASP*, **57**, 69
- Mróz, P., Udalski, A., Poleski, R., et al. 2016, *ApJS*, **222**, 9
- Schaefer, B. E. 2022, *MNRAS*, **517**, 6150
- Shafter, A. W., Ciardullo, R., & Pritchett, C. J. 2000, *ApJ*, **530**, 193
- Shafter, A. W., Curtin, C., Pritchett, C. J., Bode, M. F., & Darnley, M. J. 2014, in ASP Conf. Ser. 490, *Stellar Novae: Past and Future Decades*, ed. P. A. Woudt & V. A. R. M. Ribeiro (San Francisco, CA: ASP), 77
- Shafter, A. W., Hornoch, K., Benáček, J., et al. 2021, *ApJ*, **923**, 239
- Shafter, A. W., Kundu, A., & Henze, M. 2017, *RNAAS*, **1**, 11
- Shara, M. M. 1981, *ApJ*, **243**, 926
- Shara, M. M., Doyle, T. F., Lauer, T. R., et al. 2016, *ApJS*, **227**, 1
- Sohn, S. T., O'Connell, R. W., Kundu, A., et al. 2006, *AJ*, **131**, 866
- Stetson, P. B., 2011 DAOPHOT: Crowded-field Stellar Photometry Package, Astrophysics Source Code Library, ascl:1104.011
- Strope, R. J., Schaefer, B. E., & Henden, A. A. 2010, *AJ*, **140**, 34
- van den Bergh, S., & Younger, P. F. 1987, *A&AS*, **70**, 125
- Yaron, O., Prialnik, D., Shara, M. M., & Kovetz, A. 2005, *ApJ*, **623**, 398